

1 Assessing acetone for the GISS ModelE2.1 Earth system model

2 Alexandra Rivera¹, Kostas Tsigaridis^{2,3}, Gregory Faluvegi^{2,3}, Drew Shindell⁴

3 ¹Pratt School of Engineering, Duke University, Durham, NC, 27708, USA

4 ²Center for Climate Systems Research, Columbia University, 2880 Broadway, New York, NY, 10025, USA

5 ³NASA Goddard Institute for Space Studies, 2880 Broadway, New York, NY, 10025, USA

6 ⁴Nicholas School of the Environment, Duke University, Durham, NC, 27708, USA

7 *Correspondence to:* Kostas Tsigaridis (kostas.tsigaridis@columbia.edu)

8 **Abstract.** Acetone is an abundant volatile organic compound in the atmosphere with important influence on ozone and oxidation
9 capacity. Direct sources include anthropogenic, terrestrial vegetation, oceanic, and biomass burning emissions. Acetone is also
10 produced chemically from other volatile organic compounds. Sinks include deposition onto the land and ocean surfaces, as well as
11 chemical loss. Acetone's lifetime is long enough to allow transport and reactions with other compounds remote from its sources.
12 The latest NASA Goddard Institute for Space Studies (GISS) Earth System Model, ModelE2.1, simulates a variety of Earth system
13 interactions. Previously, acetone had a very simplistic representation in the ModelE chemical scheme. This study assesses a more
14 sophisticated acetone scheme, in which acetone is a full 3-dimensional tracer, with explicit sources, sinks and atmospheric
15 transport. We evaluate the new global acetone budget in the context of past literature. Anthropogenic emissions, vegetation
16 emissions, biomass burning, and deposition representations agree well with previous studies. Chemistry and the ocean contribute
17 to both sources and sinks of acetone, with their net values agreeing with the literature, although their individual source and sink
18 terms appear to be overestimated for chemistry and underestimated for ocean fluxes. We find the production of acetone from
19 precursor hydrocarbon oxidation has strong leverage on the overall chemical source, indicating the importance of accurate molar
20 yields for this source. Spatial distributions reveal that ocean uptake of acetone is strongest in northern latitudes, while production
21 is mainly in mid-southern latitudes. The seasonality of acetone-related processes was also studied in conjunction with field
22 measurements around the world. These comparisons show promising agreement, but have shortcomings at urban locations, since
23 the model's resolution is too coarse to capture behavior in high-emission areas. Overall, our analysis of the acetone budget aids
24 the development of this tracer in the GISS ModelE2.1, a crucial step to understanding the role of acetone in the atmosphere.

25 1 Introduction

26 Acetone (C₃H₆O) is an abundant oxygenated volatile organic compound (VOC) that has important connections to ozone and the
27 atmosphere's self-cleansing oxidation capacity (Read et al., 2012). Acetone's dynamic presence in Earth's atmosphere can be
28 described through sources, sinks, and mechanisms of transport. Extensive literature has discussed the nature of these sources and
29 sinks, and some are more well-constrained than others.

30
31 Primary sources of acetone in the atmosphere include anthropogenic, terrestrial vegetation, and biomass burning emissions. Past
32 literature has found the fluxes of these sources to range between 1-2 Tg yr⁻¹, 30-45 Tg yr⁻¹, 2.5-4.5 Tg yr⁻¹, respectively (Beale et
33 al., 2013; Brewer et al., 2017; Elias et al., 2011; Fischer et al., 2012; Folberth et al., 2006; Jacob et al., 2002; Singh et al., 2000;
34 Wang et al., 2020). Chemical production from other VOCs with 3 or more carbon atoms, each with their own molar yields, is
35 another source of acetone in the atmosphere (Brewer et al., 2017; Fischbeck et al., 2017; Hu et al., 2013; Jacob et al., 2002; Singh
36 et al., 2000; Weimer et al., 2017).

37

38 Sinks of acetone include wet and dry deposition onto the land surface, as well as chemical loss. Wet deposition occurs within and
39 below clouds due to the solubility of acetone, and depends on its Henry's Law coefficient (Benkelberg et al., 1995). Dry deposition
40 occurs on the land surface. Chemical loss of acetone forms radicals, through photolysis. Past literature has estimated the acetone
41 sinks to be 10-30% dry deposition, and 40-85% chemical loss (Arnold et al., 2005; Elias et al., 2011; Fischer et al., 2012; Khan et
42 al., 2015; Singh et al., 1994). The estimated fluxes are 10-16 Tg yr⁻¹ and 45-60 Tg yr⁻¹ for total deposition and chemical loss,
43 respectively (Arnold et al., 2005; Brewer et al., 2017; Dufour et al., 2016; Elias et al., 2011; Fischer et al., 2012; Jacob et al., 2002;
44 Khan et al., 2015; Marandino et al., 2005; Singh et al., 2000; Wang et al., 2020).

45

46 The ocean surface is a bidirectional flux that provides both a source and a sink for acetone. Ocean surface conditions such as wind
47 speed, sea surface temperature, and seawater concentration of acetone can influence the direction and magnitude of ocean-acetone
48 exchange (Wang et al., 2020). Previous literature estimates an oceanic source flux of 25–50 Tg yr⁻¹ and oceanic uptake flux of
49 35–60 Tg yr⁻¹. However, there is little consensus in the literature on whether the ocean serves as a net source or sink of acetone,
50 with some studies indicating a net oceanic source (Beale et al., 2013; Jacob et al., 2002; Wang et al., 2020), and other studies
51 indicating a net oceanic sink (Brewer et al., 2017; Elias et al., 2011; Fischer et al., 2012; Wang et al., 2020).

52

53 In addition to a global annual mean atmospheric budget, previous studies have reported the seasonality of acetone-related processes.
54 Past studies have compared monthly estimates of acetone mixing ratios to field measurements of European sites from Solberg et
55 al. (1996) (Arnold et al., 2005; Elias et al., 2011; Jacob et al., 2002). Comparisons with these European sites have emphasized the
56 seasonal variability of acetone emissions, as nearly all sites portray a summer maximum and winter minimum of acetone
57 abundance. Vegetation emissions from June to September, along with chemical sources, have an especially strong contribution to
58 this seasonality. The winter minimum of acetone is aided by an ocean sink at coastal sites (Jacob et al., 2002).

59

60 Other studies have described spatial distributions and seasonal dependence of ocean fluxes of acetone (Fischer et al., 2012; Wang
61 et al., 2020). A model by Fischer et al. (2012) proposed a net ocean sink of 2 Tg yr⁻¹ and characterized ocean uptake of acetone as
62 strongest in northern latitudes year-round, and in the high southern latitudes during the winter. An oceanic acetone source was
63 dominant in the tropical regions, with an exception off the Western coasts of Central America and Central Africa (Fischer et al.,
64 2012). A model by Wang et al. (2020) that varied surface seawater acetone concentration through a machine learning approach
65 also proposed a net ocean sink year-round. This net sink was strongest in December-February, and weakest in March-May.

66

67 The vertical distribution of acetone has been modelled between the seasons of May-October and November-April in the surface
68 and troposphere (Fischer et al., 2012). Acetone concentrations are generally higher in the lower altitudes due to proximity to surface
69 emissions. Surface-level acetone has been measured over a variety of terrestrial and oceanic sites around the world (de Gouw et
70 al., 2004; Dolgorouky et al., 2012; Galbally et al., 2007; Guérette et al., 2019; Hu et al., 2013; Huang et al., 2020; Langford et al.,
71 2010; Lewis et al., 2005; Li et al., 2019; Read et al., 2012; Schade and Goldstein, 2006; Singh et al., 2003; Solberg et al., 1996;
72 Warneke and de Gouw, 2001; Yoshino et al., 2012; Yuan et al., 2013), and in some cases, these measurements were taken over a
73 variety of months to provide a sense of seasonality (Dolgorouky et al., 2012; Hu et al., 2013; Read et al., 2012; Schade and
74 Goldstein, 2006; Solberg et al., 1996). Additionally, vertical distributions of acetone have been measured through NASA's
75 Atmospheric Tomography Mission (ATom) campaigns (Thompson et al., 2022). The ATom-1, ATom-2, ATom-3, and ATom-4
76 campaigns took place during July-August 2016, January-February 2017, September-October 2017, and April-May 2018,

Deleted: ,
Deleted: high
Deleted: ,
Deleted: which
Deleted: , either through oxidation by OH or

Deleted: ,
Deleted: ,
Deleted: strongest

85 respectively. Each campaign provided mixing ratios for a variety of VOCs in profiles from the marine boundary layer up to the
86 upper troposphere/lower stratosphere (Apel et al., 2021).

87

88 The NASA Goddard Institute for Space Studies (GISS) ModelE2.1 Earth System Model (Kelley et al., 2020) has the capability of
89 simulating a variety of Earth system interactions, is used both to interpret and predict past and future climate, and routinely
90 participates in the Climate Model Intercomparison Projects (CMIP) and Intergovernmental Panel for Climate Change (IPCC)
91 reports. Here we used [and enhanced](#) this model by adding acetone as an independent chemical tracer (Kelley et al., 2020).

Deleted: and enhanced it

92 Previously, acetone had a very simplistic representation in the model's chemical scheme (Shindell et al., 2003), in which acetone's
93 spatial variation was parameterized based on the difference of the model's zonal mean distribution of isoprene and that tracer's
94 three-dimensional distribution. Acetone's lifetime is long enough to be transported remote from sources, but not long enough to
95 become uniformly mixed, and therefore its simulated distribution should benefit from a more realistic implementation. We
96 developed a greatly improved acetone tracer scheme by making prognostic calculations of the 3-dimensional distribution of acetone
97 as a function of time. We evaluated its atmospheric burden and lifetime as well as source/sink fluxes (anthropogenic emissions,
98 vegetation emissions, biomass burning, deposition, ocean, and chemistry) against other models and its concentration against field
99 measurements. This work aims to provide a holistic assessment of the abundance of acetone in the atmosphere.

00 2 Methodology

01 [Here we implement acetone in the GISS ModelE2.1 based on the literature rather than developing a new parameterization.](#) Our
02 'Baseline' simulation is a climatological mean with year 2000 conditions, chosen to be relatively modern without precluding
03 comparison with models in older literature. The 1996-2004 mean of prescribed emissions from [Hoesly et al. \(2018\)](#) were used,
04 along with the 1996-2005 mean sea surface temperature and sea ice cover as described in Kelley et al. (2020). [Acetone simulations](#)
05 [use full chemistry and not archived OH fields.](#) An additional simulation, 'Nudged_ATOM', was conducted to compare more directly
06 with ATom field measurements. This simulation employed nudged winds (from MERRA2) (Gelaro et al., 2017) and ocean surface
07 conditions and trace gas and aerosol emissions changing with time during 2016-2018.

Deleted: ,

08 2.1 Sources

09 2.1.1 Anthropogenic emissions

10 Anthropogenic emissions were prescribed using the 1996-2004 averages of the Community Emissions Data System (CEDs)
11 emissions from Hoesly et al. (2018) as prepared for the GISS contributions to the Coupled Model Intercomparison Project, Phase
12 6 (CMIP6) (Kelley et al., 2020). These include sources from agriculture, the energy sector, the industrial sector,
13 residential/commercial/other, international shipping, solvents production and application, the transportation sector, and waste. In
14 line with past studies, we base acetone emissions on that of ketones. VOC23-ketones emissions from Hoesly et al. (2018) were
15 scaled down by a ratio of acetone molecular weight to an average ketone molecular weight ($58.08 \text{ g mol}^{-1}/75.3 \text{ g mol}^{-1}$).
16 Maintaining the resulting spatial and temporal pattern of emissions, the magnitudes were then tuned to be close to that of Fischer
17 et al. (2012), resulting in a total of about 1 Tg yr^{-1} . This resulted in roughly 36.5% of CEDs VOC23-ketones used as acetone
18 emissions. Lacking an accurate way to obtain acetone aircraft emissions from the bulk VOCs available in the emission inventory,
19 we have neglected that sector in the simulations.

Deleted: ,

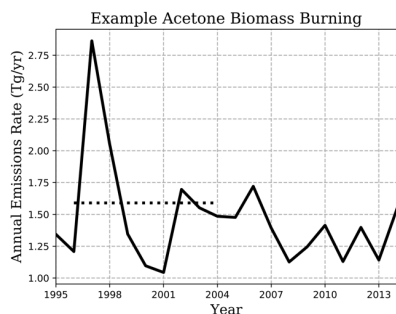
23 **2.1.2 Terrestrial vegetation emissions**

24 Emissions from land vegetation were derived from the Model Emissions of Gases and Aerosols from Nature (MEGAN), version
25 2.1 (Guenther et al., 2012), a new contribution to the ModelE. Emission response algorithms in the MEGAN2.1 model are derived
26 from input leaf area indices, solar radiation, temperature, moisture, CO₂ concentrations, and plant functional types and composition
27 of species (Guenther et al., 2012). The acetone vegetation emissions in the Baseline simulation in GISS ModelE2.1 are calculated
28 to equal 36.1 Tg yr⁻¹.

29 **2.1.3 Biomass burning emissions**

30 Acetone emissions were prescribed from a 1996-2004 average of the NMVOC-C3H6 species from version 2.1 of the biomass
31 burning dataset of van Marle et al. (2017), used by CMIP6. The acetone mass flux from biomass burning in the Baseline simulation
32 was 1.59 Tg yr⁻¹.

33
34 Figure 1 shows the biomass burning emission rate chosen for this study, and how it lies within the range of substantial interannual
35 variability. During the 20-year period shown, emissions averaged 1.463 Tg yr⁻¹, with a standard deviation of 0.402, and a spike in
36 the earlier years of emissions over 2.75 Tg yr⁻¹ is also observed (Figure 1). On top of any differences across emission inventories,
37 the years considered when reporting emissions may be the reason for variability between models (e.g. 2.40 – 2.80 Tg yr⁻¹ from the
38 2006 GFED-v2 emission inventory in Elias et al. (2011) and Fischer et al. (2012), compared to 3.22 Tg yr⁻¹ from 1997-2001 in
39 Folberth et al. (2006)).



40
41 **Figure 1.** Illustration of interannual variability of NMVOC-C3H6 biomass burning emissions of van Marle et al. (2017) (solid
42 line), used as acetone emissions in our simulation. Climatological-emissions simulations use the 1996-2004 mean (dotted line),
43 though emissions vary by month.

Deleted: with

44 **2.2 Sinks**

45 **2.2.1 Deposition**

46 Both dry and wet deposition of acetone were included in the model, although dry deposition was, on average, 91% of total
47 deposition. The wet deposition scheme is given by Koch et al. (1999). Acetone and other species are transported within and below
48 clouds, and soluble gases are deposited depending on the conditions of the grid box they are in and a Henry's Law Coefficient
49 (Shindell et al., 2001). The Henry's Law Coefficient for acetone used in the GISS ModelE2.1 is 27 mol L⁻¹ atm⁻¹, with a Henry
50 temperature dependence of acetone of 5300 J mol⁻¹ (Benkelberg et al., 1995; Zhou and Mopper, 1990). The dry deposition scheme

52 uses resistance-in-series calculations, global seasonal vegetation data (Chin et al., 1996; Shindell et al., 2001; Wesely and Hicks,
53 1977), and a reactivity factor of $f_0=0.1$. This resulted in an acetone deposition rate in the Baseline simulation of 22.2 Tg yr⁻¹.

54 2.3 Chemistry

55 The GISS ModelE2.1 Baseline simulation estimates a net chemistry change of -20.6 Tg yr⁻¹. The components can be broken up
56 into sources and sinks as follows.

57 2.3.1 Chemical sources

58 The Baseline simulation estimates chemical production to be 33.3 Tg yr⁻¹. The acetone chemical scheme includes two production
59 reactions:



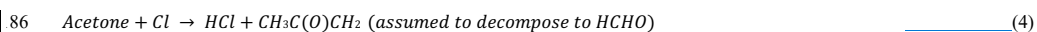
62 In the first reaction, acetone is produced by paraffin, a proxy tracer for paraffinic (saturated) carbon, and OH (Eq. 1). The molar
63 yield of acetone from paraffin was found to be a strong leverage to the overall chemical source (see Section 3.5). A rate coefficient
64 of 8.1E-13 cm³ molecule⁻¹ s⁻¹ was used (Shindell et al., 2003). Previous literature has suggested an acetone yield on a molecular
65 scale of 0.72 (Fischbeck et al., 2017; Jacob et al., 2002; Weimer et al., 2017). Initial tests using a yield of 0.72 resulted in an
66 overestimated chemistry source, leading us to re-evaluate this yield for the specific mixture of VOCs represented in the GISS
67 ModelE2.1.

68 [Our model's anthropogenic emissions of paraffin is based on an aggregation of selected VOC groups. Based on year 2019 emissions](#)
69 [of the O'Rourke et al. \(2021\) dataset, we emit paraffin that is about 11% propane by mole, 22% butane and 21% pentane.](#)
70 [Multiplying these by each VOC's acetone molar yield \(0.73, 0.95, 0.63, respectively\), we estimate that 42% of paraffin from](#)
71 [anthropogenic sources becomes acetone in our model. Paraffin biomass burning emissions, estimated from year 2020 of SSP3 70](#)
72 [emissions \(Riahi et al., 2017; Fujimori et al., 2017\) contain mole fractions for propane of 9% and higher alkanes of 23%, and when](#)
73 [multiplied by acetone molar yields of 0.73 and 0.79, respectively, suggest that about 25% of paraffin from biomass burning sources](#)
74 [becomes acetone in our model. The molar yields used in these calculations were derived with suggestions from the literature](#)
75 [\(Fischbeck et al., 2017; Jacob et al., 2002; Weimer et al., 2017\). Refer to the manuscript supplement for a more detailed breakdown.](#)
76 [Overall, an average of the 42% anthropogenic paraffin and 25% biomass burning paraffin was used to conclude that approximately](#)
77 [35% of paraffin from emissions becomes acetone, leading to our refinement of the molar yield in Eq. \(1\) to 0.35.](#)

78 Additionally, reactions between terpenes and {OH, O₃} were implemented with an acetone yield of 0.12 (Hu et al., 2013; Jacob et
79 al., 2002) (Eq. 2). The rates for these reactions are 2.51E-11*exp(444/T) cm³ molecule⁻¹ s⁻¹ for the OH reaction and 1.40E-14*exp(-
80 732/T) cm³ molecule⁻¹ s⁻¹ for the O₃ reaction, and these coefficients are enhanced from the standard α -pinene one to consider the
81 reactivity variability across mono- and higher terpenes (Tsigaridis and Kanakidou, 2003).

82 2.3.2 Chemical sinks

83 The chemical sink of acetone in the Baseline simulation is estimated to be 53.8 Tg yr⁻¹. The sinks of acetone include oxidation by
84 OH and Cl radicals, and photolysis:



Deleted: Estimated mole fractions of propane (11%), butane (22%) and pentane (21%) in anthropogenic emissions were multiplied by each compound's acetone molar yield (0.73, 0.95, 0.63, respectively), determining that 42% of paraffin from anthropogenic sources becomes acetone. Estimated mole fractions of propane (9%) and higher alkanes (23%) in biomass burning emissions were multiplied by each compound's acetone molar yield, determining that 25% of paraffin from biomass burning sources becomes acetone. The molar yields used in these calculations were derived with suggestions from the literature (Fischbeck et al., 2017; Jacob et al., 2002; Weimer et al., 2017). An average of the 42% anthropogenic paraffin and 25% biomass burning paraffin was used to conclude that approximately 35% of paraffin from emissions becomes acetone, leading to the molar yield of 0.35 in Eq. (1).



!03 The first and second acetone destruction reactions [above](#) have rates of $1.33E-13 + 3.82E-11 \cdot \exp(-2000/T)$ $cm^3 \text{ molecule}^{-1} s^{-1}$ and
!04 $7.70E-11 \cdot \exp(-1000/T)$ $cm^3 \text{ molecule}^{-1} s^{-1}$, respectively (Sander et al., 2011) (Eq. 3, 4). Previously, acetone photolysis (which only
!05 affected production of radicals and not acetone itself) did not utilize the model's photolysis scheme but was parameterized solely
!06 as a function of orbital geometry and atmospheric pressure. In the model updates, photolysis now consists of two separate reactions,
!07 where acetone forms either $CH_3CO + CH_3$ radicals or two CH_3 radicals and CO (Eq. 5, 6). Reaction 5 is pressure-dependent, while
!08 reaction 6 is temperature-dependent. [The spectroscopic data used for acetone photolysis is from JPL 2010](#) (Sander et al., 2011)
!09 [and mapped onto Fast-J version 6.8d's wavelength intervals](#) (Neu et al., 2007). [The quantum yields are pressure and temperature](#)
!10 [dependent and thus vary with altitude and location. For example, in a standard atmosphere the ratio of the yield of CO to \$CH_3CO\$](#)
!11 [decreases from 0.28 at the surface to 0.18 at 4 km altitude.](#)

!12 **2.4 Ocean**

!13 Bidirectional fluxes of acetone are calculated over ocean based on the "two-phase" model of molecular gas exchange at the air-sea
!14 interface of Liss & Slater (1974), as it is described in Johnson (2010). The fluxes are a function of simulated surface temperature
!15 and near-surface wind speed but independent of salinity. Henry's Law constants and temperature dependence of solubility for
!16 acetone are from [Sander \(1999\)](#). The atmospheric source from ocean water and sink from the atmosphere are calculated assuming
!17 a constant concentration of acetone in water (of 15 nM), the lower boundary layer atmospheric concentration, and the total transfer
!18 velocity (a combination of water-side and air-side transfer velocities). [The constant concentration of 15 nM follows the](#)
!19 [implementation by Fischer et al. \(2012\) in the GEOS-CHEM model, who looked at observations and did not find a strong reasoning](#)
!20 [to make the concentration vary seasonally or spatially.](#) The GISS ModelE2.1 Baseline simulation calculates the ocean to be a net
!21 source of acetone, producing 3.94 Tg yr⁻¹.

!22 **2.5 Sensitivity studies**

!23 Sensitivity studies were conducted to determine the influence of key parameters on the acetone budget and its global distribution
!24 ([summarized in Table 1](#)). Specifically, we were interested in seeing how much leverage a given parameter afforded the model by
!25 way of an artificial perturbation. Sensitivity studies for chemistry modify the sources of acetone. The Chem_C10 and Chem_Terp0
!26 simulations provide no formation of acetone from chlorine or terpenes, respectively. [The importance of paraffin is explored by](#)
!27 [halving its yield of acetone to 17.5% in the Chem_Par0.5 simulation, and by doubling its yield of acetone to 70% in the](#)
!28 [Chem_Par2.0 simulation.](#) As vegetation was the most prominent source, the Veg_0.7 simulation observes its reduction by
!29 [decreasing the MEGAN production of acetone by 30%.](#) The Ocn_2.0 simulation aims to explore the impact of ocean acetone
!30 [concentration by doubling it from 15 nM to 30 nM globally.](#) The Dep_f0 simulation tested dropping the reactivity factor for dry
!31 [deposition from 0.1 to zero.](#) Finally, given the high interannual variability of biomass burning emissions, the BB_2.0 simulation
!32 [explores the impact of doubling those emissions.](#)

!34 **Table 1.** Sensitivity studies conducted to observe the leverage a specific parameter afforded the model. Simulation names, as well
!35 [as the parameter they target and a description, are included.](#)

<u>GISS ModelE2.1 Sensitivity Simulation</u>	<u>Sensitivity Parameter</u>	<u>Description</u>

Deleted: (Table 1)

Deleted: (Table 1)

Deleted: (Table 1)

Deleted: (Table 1)

Deleted: (Table 1)

Moved (insertion) [1]

<u>Chem_Cl0</u>	<u>Chemistry Source</u>	<u>Acetone + Chlorine reaction rate = 0</u>
<u>Chem_Terp0</u>	<u>Chemistry Source</u>	<u>No reaction for production of acetone from terpenes</u>
<u>Chem_Par0.5</u>	<u>Chemistry Source</u>	<u>Half the yield of acetone from paraffin (17.5%)</u>
<u>Chem_Par2.0</u>	<u>Chemistry Source</u>	<u>Double the yield of acetone from paraffin (70%)</u>
<u>Veg_0.7</u>	<u>Vegetation</u>	<u>0.7 factor of acetone from MEGAN</u>
<u>Ocn_2.0</u>	<u>Ocean</u>	<u>Ocean acetone concentration from 15nM to 30nM</u>
<u>Dep_f0</u>	<u>Dry Deposition</u>	<u>f₀ changed from 0.1 to 0</u>
<u>BB_2.0</u>	<u>Biomass Burning</u>	<u>Double biomass burning emissions</u>

3 Results and model evaluation

Deleted: ¶

3.1 Global acetone budget and burden

A global acetone budget table was compiled to place our estimates in context with past global modeling studies (Table 2) (Arnold et al., 2005; Beale et al., 2013; Brewer et al., 2017; Dufour et al., 2016; Elias et al., 2011; Fischer et al., 2012; Folberth et al., 2006; Guenther et al., 2012; Jacob et al., 2002; Khan et al., 2015; Marandino et al., 2005; Singh et al., 2000, 2004; Wang et al., 2020). The values of the individual fluxes in our model (global deposition, biomass burning, anthropogenic emissions, vegetation emissions, ocean net/source/sink, and chemistry net/source/sink) were mentioned previously.

Deleted: from past global modeling studies

Table 2. Global acetone budget table comparing burden, flux and lifetime estimates of acetone from the Baseline model to thirteen previous studies.

	<u>This Study – Baseline (2021)</u>	<u>Wang et al. (2020)^a</u>	<u>Wang et al. (2020)^b</u>	<u>Brewer et al. (2017)</u>	<u>Fischer et al. (2012)</u>	<u>Elias et al. (2011)</u>	<u>Jacob et al. (2002)</u>	<u>Other Estimates (2000-2016)^c</u>
<u>Burden (Tg)</u>	<u>2.93</u>	<u>3.50</u>	<u>3.80</u>	<u>5.57</u>	<u>5.60</u>	<u>7.20</u>	<u>3.80</u>	<u>3.50 – 4.20</u>
<u>Global Deposition (Tg yr⁻¹)</u>	<u>-22.2</u>	<u>-25.2</u>	<u>-12.4</u>	<u>-12.4</u>	<u>-12.0</u>	<u>-19.0</u>	<u>-9.00</u>	<u>-26.0 – -6.0</u>
<u>Biomass Burning (Tg yr⁻¹)</u>	<u>1.59</u>	<u>4.00</u>	<u>2.40</u>	<u>2.60</u>	<u>2.80</u>	<u>2.40</u>	<u>4.50</u>	<u>3.22 – 9.0</u>
<u>Anthro Emissions (Tg yr⁻¹)</u>	<u>1.00</u>	<u>0.50</u>	<u>3.40</u>	<u>3.60</u>	<u>0.73</u>	<u>1.60</u>	<u>1.10</u>	<u>1.02 – 2.0</u>
<u>Vegetation Emissions (Tg yr⁻¹)</u>	<u>36.1</u>	<u>39.8</u>	<u>32.2</u>	<u>37.1</u>	<u>32.0</u>	<u>76.0</u>	<u>35.0</u>	<u>15 – 56</u>
<u>Net Ocean (Tg yr⁻¹)</u>	<u>3.94</u>	<u>-8.10</u>	<u>1.30</u>	<u>-7.50</u>	<u>-2.0</u>	<u>-8.0</u>	<u>13.0</u>	<u>4.00</u>
<u>— Ocean Source (Tg yr⁻¹)</u>	<u>15.2</u>	<u>33.4</u>	<u>45.7</u>	<u>51.8</u>	<u>80.0</u>	<u>20.0</u>	<u>27.0</u>	<u>20.0</u>
<u>— Ocean Sink (Tg yr⁻¹)</u>	<u>-11.3</u>	<u>-41.5</u>	<u>-44.4</u>	<u>-59.2</u>	<u>-82.0</u>	<u>-28.0</u>	<u>-14.0</u>	<u>-62.0</u>
<u>Net Chemistry (Tg yr⁻¹)</u>	<u>-20.5</u>	<u>-11.1</u>	<u>-26.1</u>	<u>-22.5</u>	<u>-21.0</u>	<u>-53.0</u>	<u>-45.0</u>	<u>-33.0 – -5.50</u>
<u>— Chem Source (Tg yr⁻¹)</u>	<u>33.3</u>	<u>38.5</u>	<u>26.1</u>	<u>24.1</u>	<u>31.0</u>	<u>27.0</u>	<u>28.0</u>	<u>15.5 – 55.6</u>
<u>— Chem Sink (Tg yr⁻¹)</u>	<u>-53.8</u>	<u>-49.6</u>	<u>-52.2</u>	<u>-46.6</u>	<u>-52.0</u>	<u>-80.0</u>	<u>-73.0</u>	<u>-61.1 – -33.4</u>
<u>Chemical Lifetime (days)^c</u>	<u>19.9</u>	<u>25.8</u>	<u>26.6</u>	<u>43.6</u>	<u>39.3</u>	<u>32.9</u>	<u>19.0</u>	<u>20.9 – 35.6</u>

Lifetime (days) ^d	12.3	11.0	12.7	17.2	14.0	21.0	14.5	12.8–35
------------------------------	------	------	------	------	------	------	------	---------

^a CAM-Chem Model (Wang et al., 2020)

^b GEOS-Chem Model (Wang et al., 2020)

^c Chemical Lifetime = Burden/Chemical Sink

^d Total Atmospheric Lifetime = Burden/Total Sink

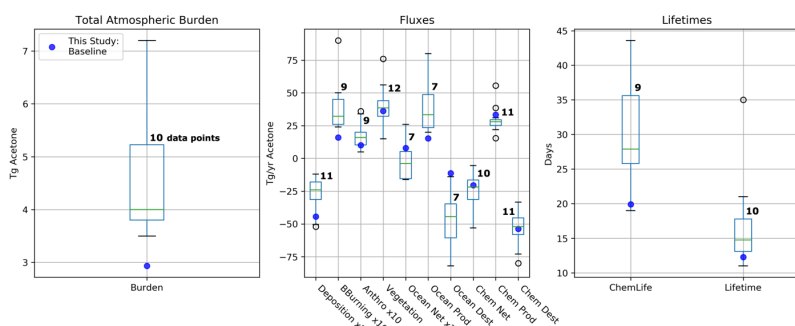
^e Singh et al. [2000, 2004], Arnold et al. [2005], Folberth et al. [2006], Marandino et al. [2006], Guenther et al. [2012], Beale et al. [2013], Khan et al. [2015], Dufour et al. [2016].

153
 154 Atmospheric burden describes the total amount of acetone that is in the atmosphere. The GISS ModelE2.1 Baseline simulation
 155 estimates the burden to be 2.93 Tg. Additionally, chemical lifetime and atmospheric lifetime can be derived from burden. The
 156 chemical lifetime of acetone is calculated as the burden divided by the chemical sink, whereas total lifetime is the burden divided
 157 by all sinks. The chemical and total atmospheric lifetimes for the Baseline simulation are calculated to be 19.9 and 12.3 days,
 158 respectively. These values are also placed in the context of previous literature in Table 2.

Deleted: yr¹

Deleted: 1

159
 160 The GISS ModelE2.1 Baseline acetone budget is further compared to previous model studies in Figure 2. The calculated fluxes in
 161 our Baseline simulation that are less than one standard deviation away from the literature mean include anthropogenic
 162 and vegetation emissions, net ocean, net chemistry, chemical production, and chemical destruction (Figure S1). Biomass burning in
 163 GISS ModelE2.1 appears as an outlier when compared against 9 previous model studies but can be attributed to the high interannual
 164 variability with emissions (as discussed in Section 2.1.3). The value of acetone deposition is on the high (more negative) end in
 165 GISS ModelE2.1 relative to 11 previous studies. This might be partially attributed to differences in deposition parametrization
 166 across models, as explored by our sensitivity study on dry deposition presented in section 3.5.2. The values for oceanic acetone
 167 sources and losses are smaller (in absolute values) than the mean from 7 previous model studies. Nevertheless, the net ocean flux
 168 matches the literature well. Lastly, the total atmospheric burden and lifetime calculated by GISS ModelE2.1 are lower than the
 169 previous papers, an expected consequence of the higher removal by deposition. The chemical lifetime is also calculated to be at
 170 the low end of published literature. As the burden is a function of many different atmospheric parameters, however, it was not the
 171 goal to corroborate our estimates with the literature as much as it was for each of the fluxes.

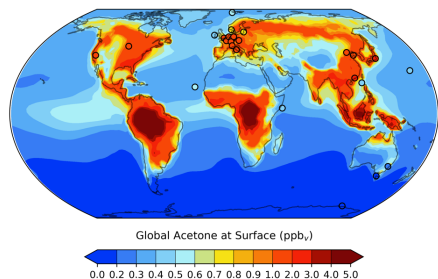


172
 173 **Figure 2.** Total atmospheric burden, fluxes, and lifetimes of acetone from the literature values in Table 2 (shown in boxes and
 174 whiskers with outliers as open circles), and values from GISS ModelE2.1 (shown as solid circles). The number of models used to
 175 create each box and whisker plot are labelled. Note that deposition and ocean net fluxes were multiplied by 2 and biomass burning
 176 and anthropogenic emissions were multiplied by 10 for a better visualization of the distribution.

Deleted: in

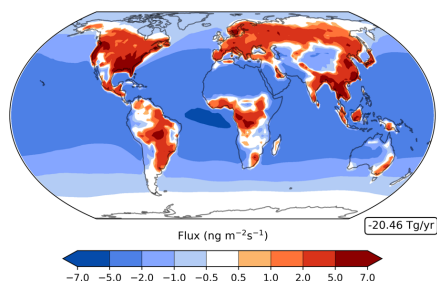
!80 **3.2 Spatial distribution of acetone**

!81 The global distribution of acetone at the surface is given in Figure 3. It is evident that acetone mixing ratios are largest over the
!82 continents, where anthropogenic, vegetation, and other terrestrial sources are located. Over the ocean, acetone mixing ratios are
!83 highest downwind of central America and central Africa. A comparison of the GISS ModelE2.1 results against twenty-six prior
!84 field measurements shows an overall great agreement, with a root mean squared error of 0.3494 and an R^2 value of 0.8306. To put
!85 these results into the context of model evaluation, a similar comparison to field measurements was done for the model's previous
!86 acetone scheme. The prior parameterization was designed as a rough representation of acetone oxidized from isoprene in the upper
!87 troposphere, without regard for realism near the surface, and this is evident from the comparison with surface observations: a root
!88 mean squared error and R^2 value of 1.3620 and 0.0413, respectively. The improvement of the new acetone tracer model in the
!89 GISS ModelE2.1 is evident from these statistics.

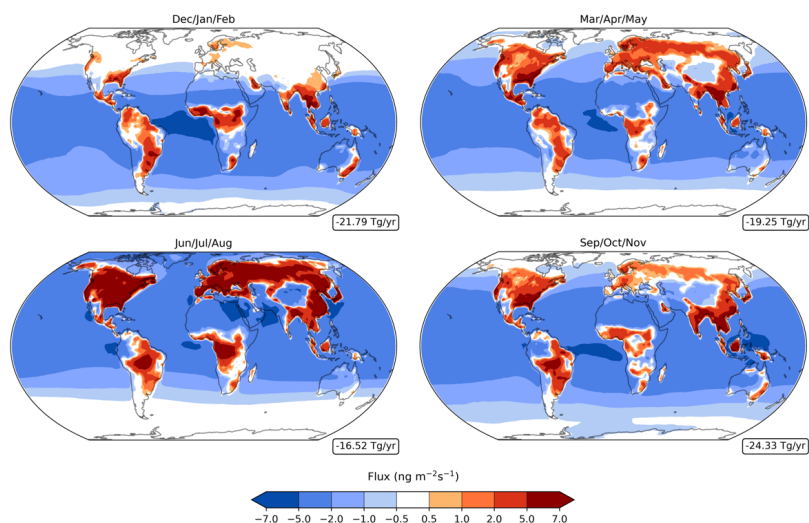


!90
!91 **Figure 3.** GISS ModelE2.1 spatial distribution of annual mean acetone at surface for the Baseline simulation. Filled circles
!92 represent data from twenty-six field measurements (de Gouw et al., 2004; Dolgorouky et al., 2012; Galbally et al., 2007; Guérette
!93 et al., 2019; Hu et al., 2013; Huang et al., 2020; Langford et al., 2010; Lewis et al., 2005; Li et al., 2019; Read et al., 2012; Schade
!94 & Goldstein, 2006; Singh et al., 2003; Solberg et al., 1996; Warneke & de Gouw, 2001; Yoshino et al., 2012; Yuan et al., 2013).
!95 The root mean squared error and the R^2 value between the Baseline acetone estimations and the field measurements are 0.3494
!96 and 0.8306, respectively. A nonlinear colorbar is used to better differentiate the details in the map.

!97
!98 A breakdown of the acetone bidirectional fluxes indicates that its chemical production is concentrated over the continents, while
!99 chemical destruction is primarily over the oceans (Figure 4). Hotspots of production over the continents include the Southern and
!00 Eastern United States and central South America, East and Northern Asia, and Central Africa. Chemical sinks over the oceans are
!01 stronger in the tropics than in the high southern or northern latitudes. Annually, there is a net negative flux of about $-20.46 \text{ Tg yr}^{-1}$
!02 (Figure 4). Observing the chemical flux over all four seasons, the net loss appears unaffected while the net source changes more
!03 significantly, following the seasonality of precursor compounds like isoprene and terpenes (Figure 5). Chemical production is
!04 strongest in the months of June/July/August, primarily in the US and Northern Asia. Production is weakest in the months of
!05 December/January/February, losing almost all production in the US and Northern Asia entirely. Still, a net negative flux is present
!06 for all four seasons (Figure 5).



107
108 **Figure 4.** Annual average of acetone net chemistry fluxes (column-integrated) in the Baseline simulation, with red indicating a net
109 source and blue indicating a net sink. A nonlinear colorbar is used to better differentiate the details in the map. The weighted global
110 mean of the net chemistry flux is shown in a box on the lower right.

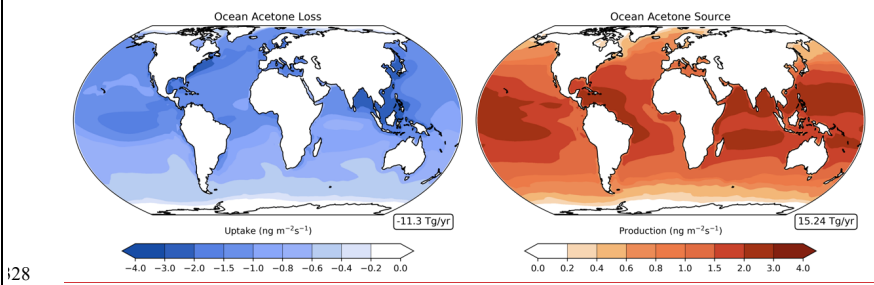


112
113 **Figure 5.** Acetone net chemistry fluxes (column-integrated) in the Baseline simulation for December-February (top left), March-
114 May (top right), June-August (bottom left), and September-November (bottom right), with red indicating a net source and blue
115 indicating a net sink. Nonlinear colorbars are used to better differentiate the details in the map. The weighted global means of the
116 net chemistry fluxes are shown in boxes on the lower right.

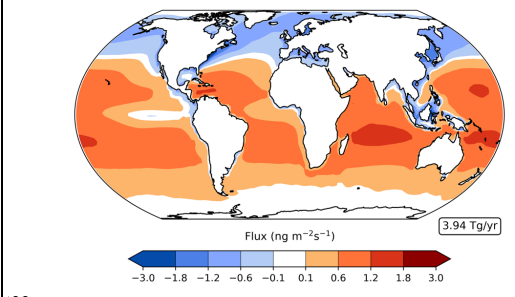
117
118 The ocean acetone sources and sinks are unevenly distributed across latitudes. Oceanic uptake of acetone is mostly concentrated
119 in the northern rather than the southern oceans, while the ocean acetone source is strongest in the tropics and decreases at higher
120 latitudes of both hemispheres (Figure 6). Combining these two unidirectional fluxes results in the ocean serving as a sink in the
121 northern high latitudes, a source in the tropical latitudes, and near neutral at the high southern latitudes (Figure 7). This finding

i22 corroborates very well with findings from Fischer et al. (2012) and Wang et al. (2020). Oceanic bidirectional acetone fluxes present
 i23 trends over the four seasons (Figure S2). Overall, every season has a positive global mean net flux. However, production becomes
 i24 strongest in the months of December through May, and weakest in the months of June through November. Off the coast of western
 i25 South America, the ocean appears to be a net sink of acetone, even though this latitude band is generally a source of acetone. This
 i26 is especially evident in the months of June/July/August and September/October/November. As the model simulates this location
 i27 to have high levels of acetone at the surface (Figure 3), we believe the acetone in the air is driving the ocean to be a sink there.

Deleted: (Figure S2)



i28 **Figure 6.** Annual average of the acetone ocean loss (left) and ocean source (right) in the Baseline simulation. Nonlinear colorbars
 i29 are used to better differentiate the details in the map. The corresponding weighted global means of the ocean fluxes are shown in
 i30 boxes on the lower right.
 i31
 i32



i33 **Figure 7.** Annual average of acetone ocean bidirectional fluxes in the Baseline simulation, with red indicating a net source and
 i34 blue indicating a net sink. A nonlinear colorbar is used to better differentiate the details in the map. The weighted global mean of
 i35 the net chemistry flux is shown in a box on the lower right.
 i36

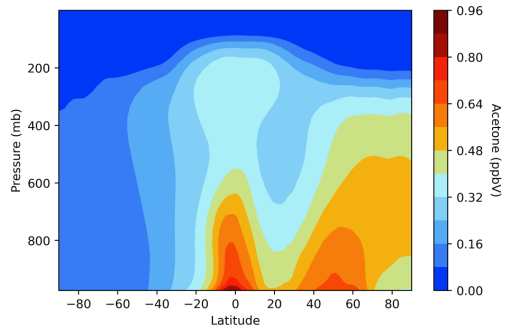
Deleted: Same as Figure 4, for the ocean bidirectional fluxes.

i37 **3.3 Vertical distribution of acetone**

i38 The vertical distribution of acetone varies by latitude, with near-surface air mixing ratios being higher in the tropics and in the
 i39 northern midlatitudes. Acetone levels in the atmosphere decrease with height, a direct result of sinks dominating the sources (Figure
 i40 8). Prior to the implementation of an acetone tracer in the GISS ModelE2.1, when acetone was derived from the zonal mean of
 i41 isoprene, the vertical distribution looked very different. Acetone was only concentrated around the tropics and did not extend

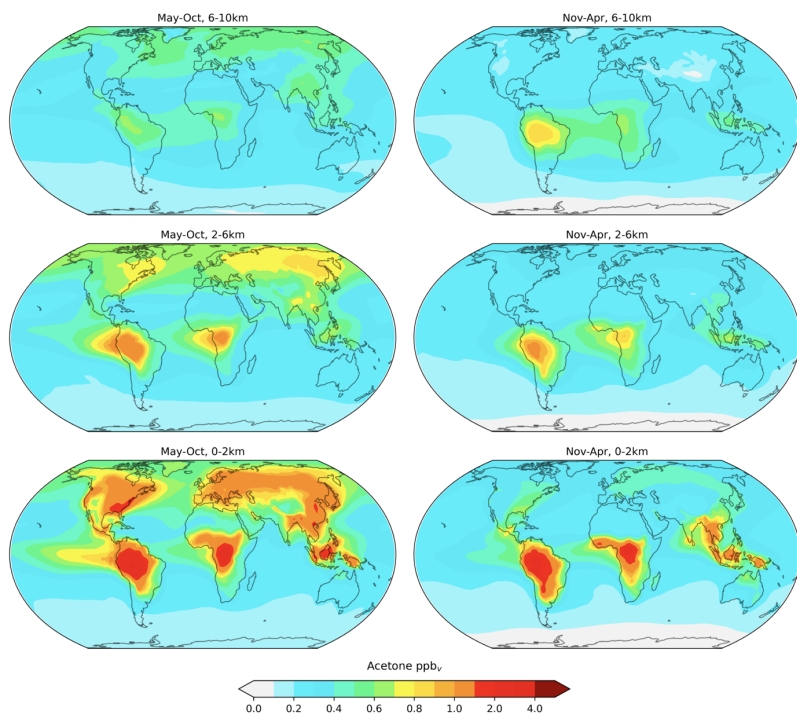
Deleted: (Figure S3)

i45 nearly as high into the atmosphere. The complexity of Figure 8 supports the new acetone tracer scheme as a significant
i46 improvement to the GISS ModelE.



i47
i48 **Figure 8.** GISS ModelE2.1 vertical distribution of acetone air mixing ratios across latitudes in the Baseline simulation.

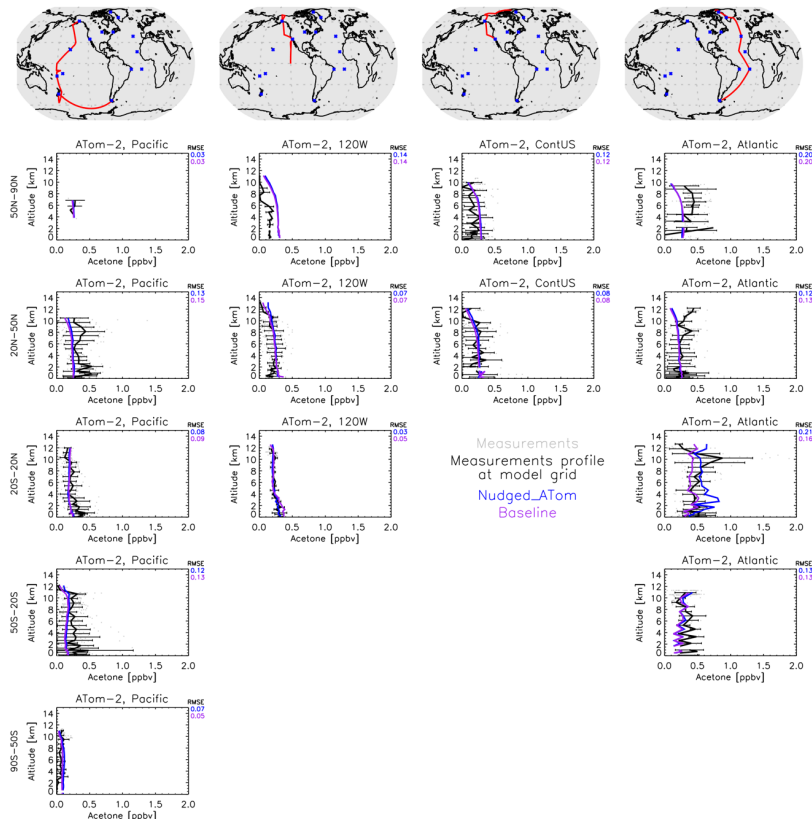
i49
i50 Another modelled vertical distribution of acetone, including a differentiation between two long seasons, is explored in Figure 9.
i51 In general, it was found that acetone mixing ratios are higher in the months of May-October than in November-April, and that this
i52 relationship is stronger in the lower atmosphere (0-2 km) than the upper atmosphere (6-10 km). This finding corroborated well
i53 with a similar analysis done by Fischer et al. (2012).



154
 155 **Figure 9.** Baseline simulation acetone mixing ratios in the atmosphere at 0-2 km (bottom), 2-6 km (middle), and 6-10 km (top) for
 156 the months of May-October (left) and November-April (right). The mixing ratios in the vertical were averaged with an arithmetic
 157 mean. The choice of the slices and colors match those in Figure 1 by (Fischer et al., 2012).

158
 159 Additionally, the GISS ModelE2.1 was compared to four ATom campaigns (Thompson et al., 2022) of acetone field measurements
 160 in the atmosphere (Apel et al., 2021). For this comparison, we averaged the flight data to the model grid, and then compared the
 161 resulting mean against the monthly mean fields of the model output. Contrary to other chemical species measured during ATom
 162 that vary significantly in space and time, acetone has a rather long lifetime, and the data are collected for the most part very far
 163 from its sources. Combining that with the fact that prescribed emissions in the model vary by month, not by day or even hour in
 164 GISS ModelE2.1, makes such a comparison appropriate. Meteorology though can affect long-range transport significantly, so for
 165 that reason we performed a nudged simulation (called Nudged_ATOM) towards the MERRA-2 reanalysis (Gelaro et al., 2017), to
 166 capture such an effect more accurately. We also used emissions and greenhouse gas concentrations from the years of the ATom
 167 campaigns and varying with year, rather than the climatological means used in the Baseline simulation. Both the Nudged_ATOM
 168 and Baseline simulations are plotted in the ATom comparisons presented here (Figure 10).

Deleted:



170

171 **Figure 10.** Comparison between the GISS ModelE2.1 simulations (Baseline in purple and Nudged_ATOM in blue) and the ATom-
 172 2 field measurements (January-February 2017). Individual data points are shown with grey dots, and their average values are shown
 173 in black, with error bars representing the one-sigma range of the averages. The root mean square error (RMSE) of each simulation
 174 is shown at the top right of each plot.

175

176 There are very few notable differences between the nudged and climatological simulations. An example is the tropical Atlantic
 177 Ocean, where during ATom-2 (Figure 10), the nudged simulation calculates higher acetone concentrations, but without gain of
 178 skill. Both model simulations miss the upper tropospheric peak that is found in the measurements, likely indicating a missing long-
 179 range transported plume. Something similar is calculated during ATom-3 (Figure S4) for the southern Atlantic Ocean mid-latitudes,
 180 where the nudged simulation is higher. Contrary to the ATom-2 case, both simulations calculate an upper tropospheric maximum,
 181 which is not found in the measurements. The tropical and southern mid-latitude Atlantic Ocean regions are both downwind African
 182 biomass burning regions during ATom-2 and ATom-3, respectively, hinting to a primary and/or secondary incorrect source of
 183 acetone related with biomass burning and subsequent long-range transport. Other than those few cases, for the most part the two
 184 simulations are indistinguishable, indicating that our conclusions comparing climatological simulations to ATom should be robust.

(Figures 10, and S3-S5). This is important to remember in Section 3.5.3, where we perform sensitivity analyses using climatological simulations and comparing against all four ATom campaigns.

3.4 Seasonality of acetone

Most European sites presented in Figure 3 have monthly-resolved measurements that can be used to analyze the seasonal behavior of acetone in the model (Figure 11, Figure S6) (Solberg et al., 1996). These sites differ with respect to their geographic locations and their proximity to anthropogenic sources. Zeppelin, Birkenes, Rucava, and Mace Head are all coastal sites, while Waldhof, Kosetice, Donon, Ispra, and Montelibretti are inland sites. Regarding anthropogenic sources, Zeppelin is the most remote location and Birkenes and Rucava each have small sources. Mace Head is a site affected by the marine boundary layer, and Waldhof, Kosetice and Donon are sites with small local anthropogenic sources that are generally located in higher emission regions. Montelibretti and particularly Ispra are subject to the highest anthropogenic sources. The measurements taken at Ispra show an opposite seasonality than what is expected, and previous studies have considered this anomalous (Jacob et al., 2002).

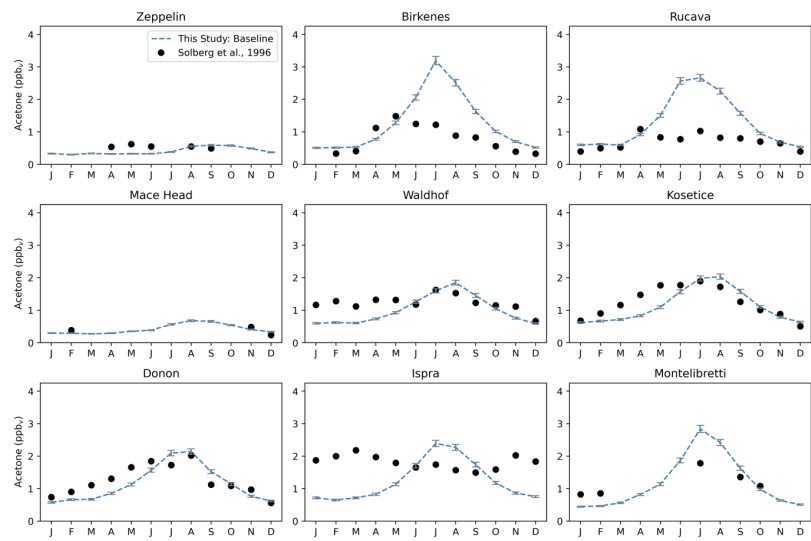


Figure 11. Acetone over twelve months at nine European sites, similar to that of Jacob et al. (2002). The modelled estimates of acetone at the surface from the Baseline simulation are shown as dashed blue lines and the grey error bars represent the one-sigma range of the modelled concentrations in the climatological mean of 5 years. Field measurements from Solberg et al., (1996) are shown as solid black dots. Root mean squared error between the Baseline simulation and field measurements are (left to right, top to bottom): 0.1968, 0.8714, 0.8724, 0.0914, 0.3907, 0.3430, 0.3160, 0.9454, 0.5454.

The GISS ModelE2.1 matches the seasonality of the measurements especially well in Zeppelin, Mace Head, Waldhof, Kosetice, and Donon; the average root mean square error between the Baseline model and the measurements at these five sites are 0.27. The Baseline model overestimates the measurements in Birkenes and Rucava (RMSE \cong 0.87 for both), even though these two sites have low anthropogenic sources. This overestimation has been attributed to the vegetation source, which has a distinct seasonality

Deleted: Although there are some differences at times, for example in the tropical Atlantic Ocean, for the most part the two simulations are indistinguishable, indicating that our conclusions comparing climatological simulations to ATom should be robust. (Figure 10, Figures S4-S6). The GISS ModelE2.1 was found to match measurements particularly well in the winter and fall seasons (ATom-2 and ATom-3, respectively). The model underestimated measurements in the mid-northern latitudes in the spring and summer seasons (ATom-4 and ATom-1, respectively), indicating that perhaps the model is not capturing a spring/summer source of acetone in the North. Generally, however, the model matches remote atmosphere measurements remarkably well (Figure 10, Figures S4-S6)....

Deleted: S7

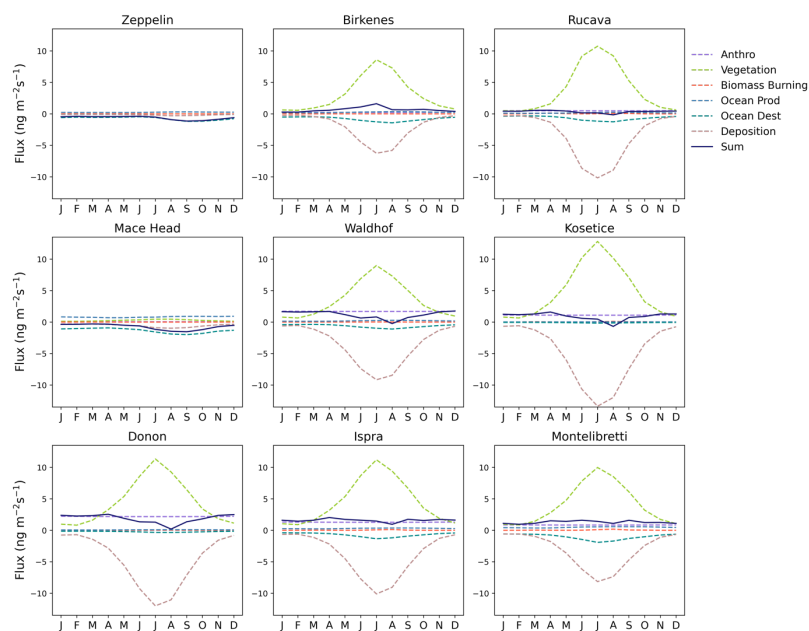
Deleted: , especially

Deleted: .

Deleted: The root mean squared error (RMSE) between the Baseline model and measurements at these five sites are 0.1969, 0.0914, 0.3907, 0.3430 and 0.3160, respectively.

127 and is much stronger than any other source there. Interestingly, in Montelibretti, the model's overestimation of vegetation, yet
128 underestimation of local emissions, results in a decent estimation of the sources there (RMSE = 0.5454) (Figure 11).

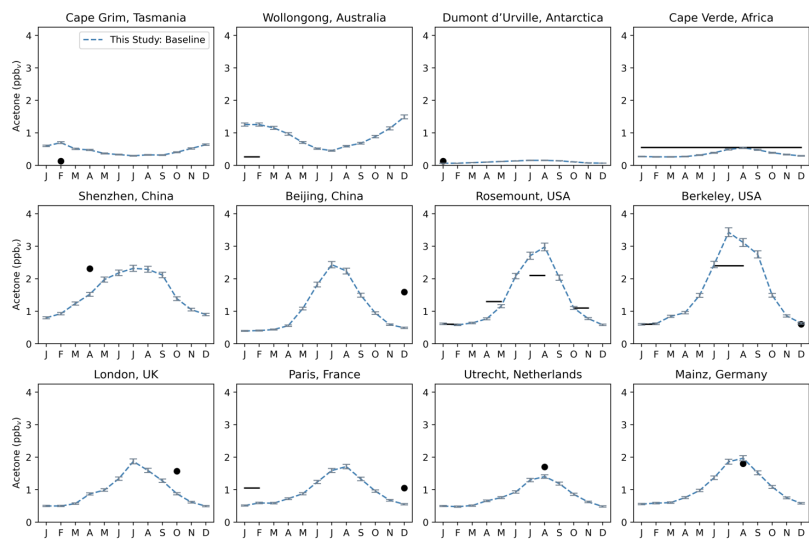
129
130 As mentioned previously, an analysis of the distribution of the regional sources and sinks at the nine European sites shows that,
131 except for Zeppelin and Mace Head, all studied European sites have vegetation as the dominant source that strongly contributes to
132 the simulated seasonality of concentrations (Figure 12). Vegetation sources peak in the summer months and are lower in the winter.
133 Deposition is a major sink of acetone that is comparable in magnitude with the vegetation source. Ocean uptake of acetone follows
134 a weak seasonal cycle, being stronger in the summer months. The other fluxes (anthropogenic emissions, biomass burning and
135 ocean production) do not exhibit much seasonality at these locations (Figure 12).



136
137 **Figure 12.** Contribution of acetone sources and sinks in the Baseline simulation over twelve months on the regional level (10° x
138 12.5° grid boxes) at nine European sites. The sources and sinks are shown as various colored dashed lines, and their sums are
139 shown as a solid navy-blue lines.

140
141 We also compared the GISS ModelE2.1's surface acetone at observation sites with less temporal coverage (Figure 13). In general,
142 the GISS ModelE2.1 matches the field measurements well. This is especially true for the non-summer seasons in Rosemount and
143 Berkeley, and the summer peaks in Utrecht and Mainz. The model seems to be overestimating acetone around Australia, as shown
144 by comparisons with Cape Grim and Wollongong, while underestimating emissions in large cities like Shenzhen, Beijing, London,
145 and Paris.

Deleted: ¶
Deleted: (de Gouw et al., 2004; Dolgorouky et al., 2012; Galbally et al., 2007; Guérette et al., 2019; Hu et al., 2013; Huang et al., 2020; Langford et al., 2010; Legrand et al., 2012; Li et al., 2019; Read et al., 2012; Schade and Goldstein, 2006)



151 **Figure 13.** Acetone over twelve months for various sites that do not have enough measurements to resolve seasonality (Australia, 152 Antarctica, Africa, Asia, Europe, North America). The modelled estimates of acetone at the surface from the Baseline simulation 153 are shown as dashed blue lines and the grey error bars represent the one-sigma range of the modelled concentrations in the 154 climatological mean of 5 years. The modelled estimates are overlaid with monthly (solid circles) or seasonal (solid lines) field 155 measurements, as found in the literature (de Gouw et al., 2004; Dolgorouky et al., 2012; Galbally et al., 2007; Guérette et al., 2019; 156 Hu et al., 2013; Huang et al., 2020; Langford et al., 2010; Legrand et al., 2012; Li et al., 2019; Read et al., 2012; Schade and 157 Goldstein, 2006). 158

159 3.5 Sensitivity studies

160 The sensitivity simulations presented here have been described in section 2.5 and in Table 1. We grouped them in two categories: 161 those directly related with chemical sources and sinks, and those related with terrestrial and oceanic acetone fluxes. Overall, the 162 sensitivity studies that presented large changes to total atmospheric burden included Chem_Terp0, Chem_Par0.5, Chem_Par2.0, 163 Veg_0.7, Ocn_2.0, and Dep_f0 (all but Chem_Cl0 and BB_2.0) (Figures S7-S12).

164 3.5.1 Chemistry

165 Chemistry sensitivity tests that modified the sources of acetone were analyzed with respect to the budget and global distribution 166 of acetone. In the Chem_Cl0 simulation, where no acetone oxidation by the chlorine radical occurs, the overall global acetone 167 budget does not change. However, in some places like Rucava, Ispra, Montelibretti, and Shenzhen, the shape of the acetone 168 concentration profile over the year changes slightly (Figure 14, Figure S13). The Chem_Terp0 simulation that removes the 169 production of acetone from terpenes decreases the summer peak of acetone by as much as 35.5% in Birkenes, 25.5% in Mainz, 170 and 25.3% in Berkeley (Figure 14, Figure S13). Other sites like Montelibretti, Ispra and Paris have their summer peak decreased 171 by 22.6%, 22.2%, and 19.0%, respectively (Figure 14, Figure S13). Coastal and remote areas like Zeppelin, Mace Head and 172 Dumont d'Urville are not impacted by the removal of terpenes (Figure 14, Figure S13). There seems to be some nonlinearities

Deleted: S8

Deleted: S13

Deleted: S14

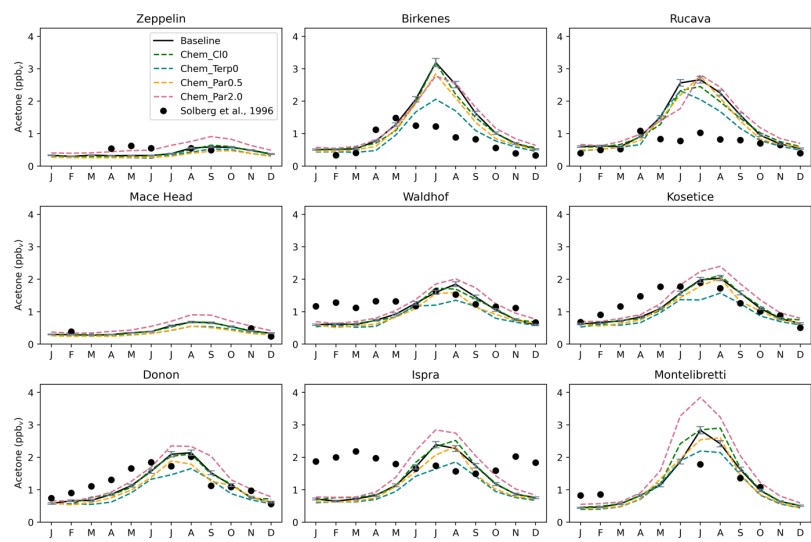
Deleted: 4

Deleted: 4

Deleted: 4

179 with the relationship between acetone abundance and its yield from paraffin, as the results from the Chem_Par2.0 and Chem_Par0.5
 180 simulation reveal that doubling the yield has a stronger impact than halving it. For instance, in Montelibretti, doubling the yield
 181 from paraffin increases the summer peak by 35.7%, while halving the yield decreases the summer peak by only 8.3% (Figure 14,
 182 Figure S13). A similar relationship is observed at other sites: Ispra (19.1% increase with double paraffin, 2.5% decrease with half
 183 paraffin) and Berkeley (12.7% increase with double paraffin, 2.5% decrease with half paraffin) (Figure 14, Figure S13). Overall,
 184 we explored chemistry sensitivities that would tend to push acetone in both directions. The Baseline simulation falls between our
 185 tests, which we have identified as important uncertainties.

Deleted: 4
 Deleted: 4



186 **Figure 14.** Similar to Figure 11, but with the chemistry sensitivity studies added. The modelled estimates of acetone at the surface
 187 from the Baseline simulation are shown as solid black lines, and the sensitivity studies are as follows: removing the acetone +
 188 chlorine reaction (dashed green lines), removing the production of acetone from terpenes (dashed blue lines), halving the yield of
 189 acetone from paraffin (dashed orange lines), and doubling the yield of acetone from paraffin (dashed pink lines). Field
 190 measurements from Solberg et al., (1996) are shown as solid black dots.

192 The spatial distribution differences between the chemistry sensitivity studies and the Baseline simulation show some interesting
 193 patterns (Figure 15). Removing the production of acetone from terpenes oxidation decreased acetone over the continents, and
 194 especially over tropical and boreal forests which are where terpenes are emitted. This change induced a feedback where acetone
 195 concentration increased slightly over the oceans (Figure 15, top left). Halving production of acetone from paraffin oxidation only
 196 decreased acetone concentrations over the continents (Figure 15, top right), while doubling it increased acetone concentrations
 197 over the continents but reduced it marginally downwind (Figure 15, bottom). Feedback resulting from this change was that acetone
 198 destruction increased over the tropics.
 199

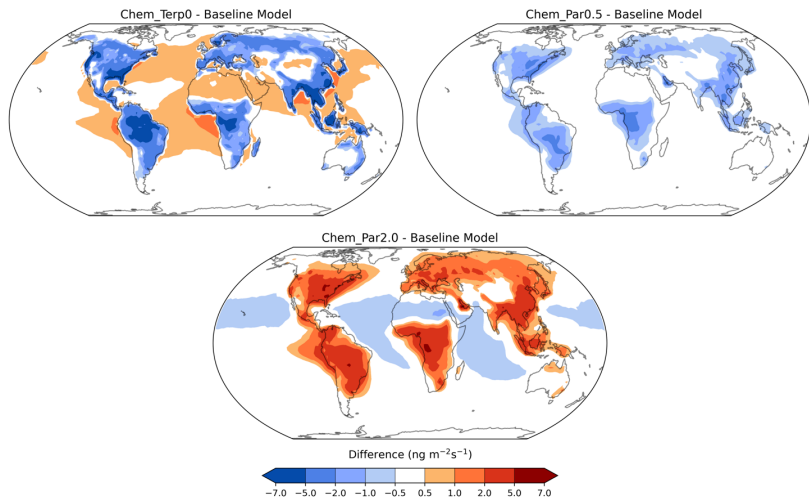


Figure 15. Chemistry sensitivities anomalies from Baseline, with red indicating an increase and blue indicating a decrease of the column-integrated net acetone chemistry flux. Nonlinear colorbars are used to better differentiate the details in the map. The fourth chemistry sensitivity study, Chem_ClO, is omitted, since the changes everywhere are very small, less than $0.4 \text{ ng m}^{-2} \text{ s}^{-1}$.

3.5.2 Terrestrial and oceanic fluxes

Terrestrial and oceanic fluxes sensitivities were analyzed at the same sites. The vegetation flux sensitivity, Veg_0.7, reduced acetone production from MEGAN by 30%. This change decreased the summer peak of acetone down at nearly every location studied, but most notably by 32.6% in Birkenes, 22.9% in Rucava, and 22.2% in Rosemount (Figure 16, Figure S14).

Deleted: 5

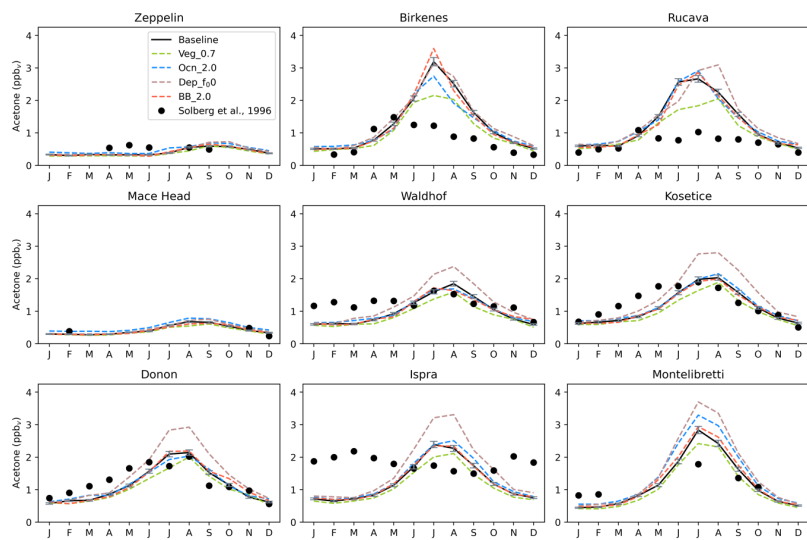


Figure 16. Similar to Figure 11, but with the terrestrial and oceanic sensitivity studies added. The modelled estimates of acetone at the surface from the Baseline simulation are shown as solid black lines, and the sensitivity studies are as follows: reducing vegetation emissions to 0.7 acetone from MEGAN (dashed light-green line), doubling ocean acetone concentration (dashed blue line), changing the reactivity factor for dry deposition (dashed brown line), and doubling biomass burning emissions (dashed orange line). Field measurements from Solberg et al., (1996) are shown as solid black dots.

In the oceanic flux sensitivity simulation, Ocn_2.0, the concentration of acetone in the water was doubled from 15 nM to 30 nM. The results of this simulation varied with geographic location. For instance, in Birkenes, doubling ocean concentration reduced overall acetone by 13.9%, while in Montelibretti, it was increased by 16.1% (Figure 16). Even though Birkenes is more of a coastal city than Montelibretti, this result may simply be a temperature effect; Birkenes is at 58°N, while Montelibretti is at 42°N, and a warmer ocean may produce more acetone. Overall, in most places, the doubling ocean acetone concentration did not change much atmospheric acetone throughout the year.

Another broader finding from the ocean sensitivity study is that doubling the ocean acetone concentration impacted oceanic emissions of acetone more than the oceanic uptake of acetone. Specifically, in this sensitivity study the emissions doubled while the uptake only increased by 40%. This difference may be attributed to the fact that a higher ocean concentration will generally cause less resistance in the emission direction, but more resistance in the uptake direction. The differences in oceanic acetone emissions and uptakes in this sensitivity study also resulted in increased chemical destruction, and an overall higher burden of acetone in the atmosphere (Figure S11).

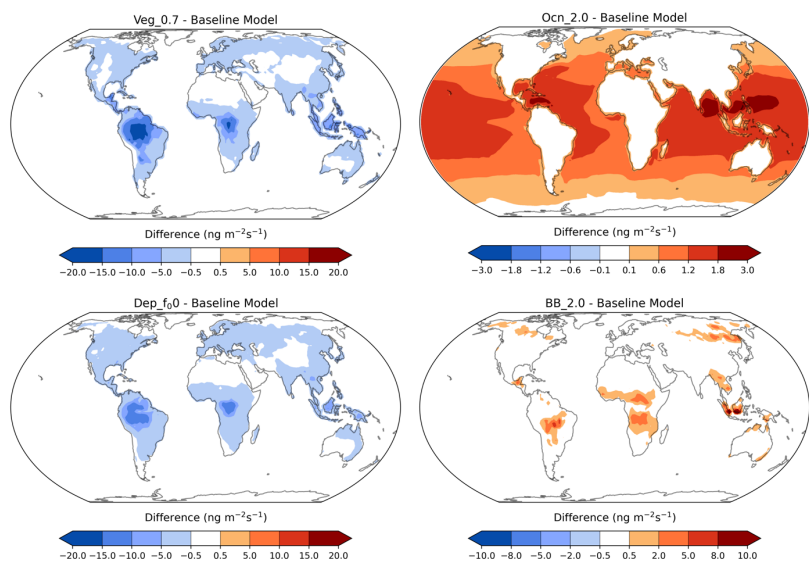
In the dry deposition sensitivity simulation, the reactivity factor, f_0 , was reduced from 0.1 to 0. As a result, the amount of acetone removed by deposition decreased, and the atmospheric acetone concentration increased. The strongest increases were found to be in Ispra (38.4% increase), Kosetice (37.9% increase), Paris (37.9% increase), Beijing (37.3% increase), Donon (36.6% increase),

Deleted: ,

Deleted: S12

i37 Mainz (33.4% increase), Montelibretti (30.5% increase), Rosemount (28.9% increase), Berkeley (28.7% increase), and Waldhof
i38 (28.7% increase) (Figure 16, Figure S14). The final terrestrial fluxes sensitivity study, BB 2.0, doubled biomass burning emissions.
i39 This sensitivity did not significantly change acetone mixing ratios in any of the locations studied, except an increased summer
i40 spike (12.7% increase) in Birkenes (Figure 16). Most of the locations studied were far from biomass burning sites to begin with,
i41 however, so an analysis of this sensitivity study over biomass burning hotspots is needed.

i42
i43 The acetone concentration anomalies around the world between the terrestrial and oceanic fluxes sensitivity studies and the
i44 Baseline simulation are presented in Figure 17. Decreasing acetone production from MEGAN vegetation by 30% resulted in a
i45 decrease of acetone mixing ratios over the tropical and boreal forests, where this source is most prominent (Figure 17, top left).
i46 Doubling ocean acetone concentrations increased production of acetone from the oceans globally. This increase was stronger in
i47 the tropics, due to the higher sea surface temperatures (Figure 17, top right). Reducing the reactivity factor for dry deposition
i48 decreased the amount of acetone removed by deposition over the continents (Figure 17, bottom left), in particular where acetone
i49 concentration is elevated (Figure 3). Finally, doubling biomass burning emissions did not change acetone mixing ratios much,
i50 other than over biomass burning hotspots like central South America, central Africa, Southeast Asia, and Siberia (Figure 17, bottom
i51 right).



i52
i53 **Figure 17.** Acetone anomalies from the Baseline simulation for the vegetation (top left), ocean (top right), dry deposition (bottom
i54 left) and biomass burning (bottom right) sensitivities, with red indicating an increase and blue indicating a decrease of the specific
i55 flux. Nonlinear colorbars are used to better differentiate the details in the map.

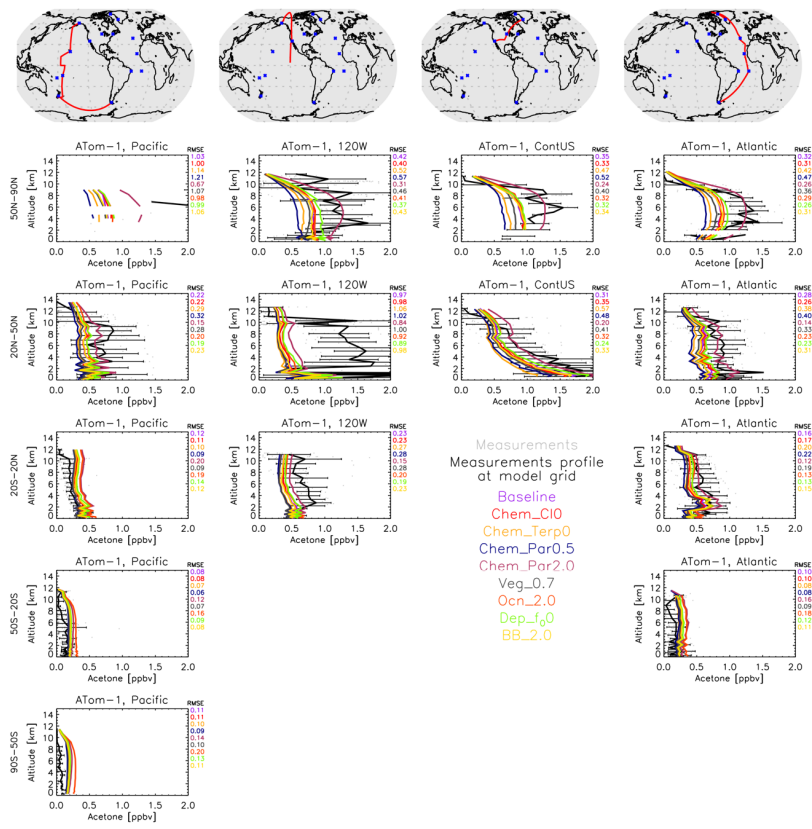
i56 3.5.3 A_{Tom} comparisons

i57 The A_{Tom} comparisons were replicated with the sensitivity simulations (Figure 18, Figures S15-S17). Doubling the paraffin
i58 yield of acetone seemed to have the most noticeable impacts on the vertical profiles. As seen during A_{Tom}-1 (July-August

Deleted: 4

Deleted: The A_{Tom} comparisons were replicated with the sensitivity simulations (Figure 18, Figures S16-S18). Doubling the paraffin yield and doubling the ocean acetone concentration seemed to have the most noticeable impacts on the vertical profiles. As seen in the summer season (A_{Tom}-1), doubling the paraffin yield more closely matches the measurements in the Northern hemisphere remote atmosphere (Figure 18). In the fall season (A_{Tom}-3), however, doubling the paraffin yield tends to overshoot most of the measurements (Figure S17). These results reveal that the model may be missing a paraffin source that is active during the summer season, and a paraffin sink that is active in the fall season. Additionally, the ocean sensitivity tends to shift the vertical profile right (overshooting measurements) in nearly all locations of the winter season (A_{Tom}-2), and in the Southern hemisphere of the other seasons. While the ocean flux may be small, these A_{Tom} comparisons reveal that they especially matter in the southern latitudes. These are the same latitudes where the ocean appears to be in equilibrium (neither a strong source nor sink) (Figure 7).

178 [2016](#), doubling the paraffin yield decreases the root mean square error (RMSE) against measurements in the Northern
 179 [hemisphere polar atmosphere](#) (Figure 18) and brings the model to closer agreement to observations, but decreases the agreement
 180 [throughout the remote Pacific Ocean, which implies different chemical formation pathways over the more polluted northern](#)
 181 [hemisphere on the Atlantic Ocean side, compared to the Pacific Ocean. Nearly the exact opposite is calculated in the case of the](#)
 182 [halving of the paraffin yield of acetone, which adds confidence to the chemical pathway explanation. The doubling of the ocean](#)
 183 [acetone concentration shows a small improvement \(decrease\) in the RMSE over the tropical and north Atlantic Ocean during](#)
 184 [ATom-1 and an even smaller decrease over the north hemisphere Pacific Ocean, but an increase over the tropical and south](#)
 185 [Pacific Ocean, showing the potential role of different ocean concentrations of acetone across the globe. It needs to be noted](#)
 186 [though that the model performs fairly well in those regions already, so the small improvements mentioned do not largely affect](#)
 187 [the regional acetone concentrations, as also expected due to the rather weak acetone source from the ocean.](#)



188
 189 **Figure 18.** Similar to Figure 10, except a comparison between the GISS ModelE2.1 sensitivity simulations and the ATom-1 aircraft
 190 measurements (July-August 2016). Individual data points are shown with grey dots, and their average values are shown in black,
 191 with error bars representing the one-sigma range of the averages. The root mean square error (RMSE) of each simulation is shown

i92 [at the top right of each plot. Note that all sensitivities are to be compared against the Baseline simulation, not the Nudged ATom](#)
i93 [one, but as shown earlier this makes very little difference in the comparison with observations \(Figure 10\).](#)

i94
i95 [The simulations of the boreal winter \(January-February 2017\) score the best against ATom-2. Acetone concentrations are the](#)
i96 [lowest during that period in both hemispheres, a direct result from the very low biomass burning emissions, which is among the](#)
i97 [highest acetone sources worldwide \(Figure 2\). In the region north of 50N, the increase of both the paraffin source and the](#)
i98 [oceanic source of acetone degrade the simulations, and the same applies for the measurements around 102W longitude,](#)
i99 [especially at mid-latitudes. The increase in oceanic source over the northern hemisphere mid-latitude Pacific Ocean improves](#)
i100 [\(decreases\) RMSE, but as already mentioned the low concentrations of acetone in that area \(and in general during ATom-2\)](#)
i101 [show that there is small sensitivity in the modified acetone sources to acetone profiles. While the ocean flux may be small, these](#)
i102 [ATom comparisons reveal that they especially matter in the southern latitudes. These are the same latitudes where the ocean](#)
i103 [appears to be in equilibrium \(neither a strong source nor sink\) \(Figure 7\).](#)

i104
i105 [During boreal fall \(ATom-3\), doubling the paraffin yield tends to overshoot most of the measurements \(Figure S16\), contrary to](#)
i106 [what was calculated during boreal summer \(ATom-1; Figure 18\). This is the case for most ATom-3 Atlantic Ocean flights, while](#)
i107 [an improvement is calculated when comparing with the flights near the west coast of the US or the Pacific Ocean mid-latitudes.](#)
i108 [These results reveal that the model may be underestimating a paraffin source during boreal summer, which diminishes during](#)
i109 [boreal fall.](#)

i110
i111 [The boreal spring season \(April-May 2018; ATom-4; Figure S17\) is the hardest for the model to simulate when it comes to](#)
i112 [northern hemisphere concentrations. All sensitivity studies greatly underestimate measurements, in particular the long-range](#)
i113 [transport upper tropospheric amount near the polar latitudes but also the concentrations measured throughout the troposphere at](#)
i114 [northern mid-latitudes. The model skillfully simulates tropical and southern hemisphere profiles, while it cannot reproduce the](#)
i115 [higher concentrations at northern latitudes. The increased yield from paraffin or the increased oceanic concentration do reduce](#)
i116 [RMSE, but still fall short on capturing the magnitude, or the shape, of the profiles of the spring hemisphere. We cannot infer](#)
i117 [from our model simulations whether this is a missing source or an underestimated sink, but the latter appears to be more](#)
i118 [plausible, given the large underestimation of all modeled profiles at northern mid-latitudes. In the southern hemisphere, the](#)
i119 [increase of oceanic acetone clearly degrades model skill, as was frequently the case during the other campaigns presented above.](#)
i120 [It is worth mentioning that for most cases the changes in the source of acetone do not alter the shape of the vertical profile. This](#)
i121 [means that the transport or chemical sinks of acetone dictate its spatiotemporal distribution more than sources, while the sources](#)
i122 [do affect the magnitude of that distribution, quite significantly under some of the conditions described here](#)

i23 **4 Conclusion**

i24 The development of acetone's representation in the NASA GISS ModelE2.1 from its previous simplistic parameterization of
i25 instantaneous isoprene to a full tracer experiencing transport, chemistry, emissions, and deposition of its own, marks a significant
i26 improvement to the model's chemical scheme. Calculations of the 3-dimensional distribution of acetone as a function of time, as
i27 well as evaluations of its atmospheric burden and source/sink fluxes demonstrate the complexity of acetone's spatiotemporal
i28 distribution in the atmosphere. An extensive analysis was conducted to assess the simulated global acetone budget in the context
i29 of past modeling studies. Further comparisons were made against field measurements on a variety of spatial and temporal scales,

i30 which indicated that the model agrees well with surface field measurements and vertical profiles in the remote atmosphere. The
i31 chemical formation of acetone from precursor compounds such as paraffin was found to be an uncertain yet impactful factor.
i32 Vegetation fluxes as calculated by MEGAN were identified as the dominant acetone source which dictates its seasonality.
i33 Additionally, the acetone concentration in seawater was found to affect oceanic sources more than oceanic sinks.

i34

i35 The work presented here demonstrates the usefulness of the approach to evaluate a chemical species in the model, and can be used
i36 for similar evaluations of other important gaseous and aerosol species. Any feedback between acetone and the rest of the chemistry,
i37 and particularly ozone, have not been assessed here, and should be the goal of a future study. Additionally, the current ocean-
i38 acetone interaction uses a constant concentration of acetone in the ocean. It will be helpful to test a more realistic, non-uniform
i39 ocean acetone concentration, when this becomes available. Finally, other atmospheric conditions such as surface wind speed may
i40 be considered further when modifying the ocean scheme.

Deleted: ,

i41 **Code Availability**

i42 The GISS ModelE code is publicly available at <https://simplex.giss.nasa.gov/snapshots/>. The most recent public version is E.2.1.2;
i43 the version of the code used here is already committed in the non-public-facing repository and will be released in the future
i44 following the regular release cycle of ModelE, under version E3.1.

i45 **Data Availability**

i46 The 3-dimensional model output of acetone concentrations will be made public at the GISS website at the time of publication in
i47 the discussion phase, as was done in other publications (e.g. <https://pubs.giss.nasa.gov/abs/ba08500g.html>). This statement will be
i48 modified accordingly for final publication.

i49

i50 We have made available the simulated three-dimensional distributions of acetone from each simulation described in the paper
i51 (Baseline, sensitivity simulations in Table 1, and Nudged_ATom). These are found in zip files, grouped by simulation, here:
i52 <https://doi.org/10.5281/zenodo.7567614>. Each zip file contains a series of netCDF format files with filenames
i53 {month}_5yrAvg_Acetone_{simulation}.nc, where each file is a climatological average over 5 years of repeated forcing
i54 conditions.

i55

i56 The exception is the transient-forcing simulation "Nudged_ATom", which contains single-month averages of acetone from JUL
i57 2016 through MAY 2018, to cover the ATom observational period. The file names for that simulation are of the form:
i58 {month}_{year}_Acetone_Nudged_ATom.nc. Acetone is in ppb, units and given on the model's native grid and vertical levels.
i59 These are hybrid sigma levels, but nominal pressure middles and edges are given in the plm and ple variables, respectively, and
i60 the grid box surface areas are also provided.

Formatted: Subscript

i61 **Author Contribution**

i62 KT conceived the study and guided the model development which was done by GF. All simulations presented here were performed
i63 by GF. DS advised during the whole development process. AR did the literature search and all comparisons against other modeling
i64 studies. With the exception of the ATom analysis and plots which were done by KT, and comparisons against field measurements

566 and the rest of the plots were done by AR. AR drafted the first version of the manuscript, and all authors contributed to it. GF
567 prepared all model outputs for dissemination.

568 **Competing Interests**

569 The authors declare that they have no conflict of interest.

570 **Acknowledgements**

571 Climate modeling at GISS is supported by the NASA Modeling, Analysis and Prediction program. AR acknowledges support from
572 North Carolina Space Grant and the NASA Office of STEM Engagement. Resources supporting this work were provided by the
573 NASA High-End Computing (HEC) Program through the NASA Center for Climate Simulation (NCCS) at Goddard Space Flight
574 Center.

575 **References**

- 576 Apel, E. C., Asher, E. C., Hills, A. J., and Hornbrook, R. S.: ATom: Volatile Organic Compounds (VOCs) from the TOGA
577 instrument, Version 2, ORNL DAAC, <https://doi.org/10.3334/ORNLDAAC/1936>, 2021.
- 578 Arnold, S. R., Chipperfield, M. P., and Blitz, M. A.: A three-dimensional model study of the effect of new temperature-dependent
579 quantum yields for acetone photolysis, *J. Geophys. Res. Atmospheres*, 110, <https://doi.org/10.1029/2005JD005998>, 2005.
- 580 Beale, R., Dixon, J. L., Arnold, S. R., Liss, P. S., and Nightingale, P. D.: Methanol, acetaldehyde, and acetone in the surface waters
581 of the Atlantic Ocean, *J. Geophys. Res. Oceans*, 118, 5412–5425, <https://doi.org/10.1002/jgrc.20322>, 2013.
- 582 Benkelberg, H.-J., Hamm, S., and Warneck, P.: Henry's law coefficients for aqueous solutions of acetone, acetaldehyde and
583 acetonitrile, and equilibrium constants for the addition compounds of acetone and acetaldehyde with bisulfite, *J. Atmospheric*
584 *Chem.*, 20, 17–34, <https://doi.org/10.1007/BF01099916>, 1995.
- 585 Brewer, J. F., Bishop, M., Kelp, M., Keller, C. A., Ravishankara, A. R., and Fischer, E. V.: A sensitivity analysis of key natural
586 factors in the modeled global acetone budget, *J. Geophys. Res. Atmospheres*, 122, 2043–2058,
587 <https://doi.org/10.1002/2016JD025935>, 2017.
- 588 Chin, M., Jacob, D. J., Gardner, G. M., Foreman-Fowler, M. S., Spiro, P. A., and Savoie, D. L.: A global three-dimensional model
589 of tropospheric sulfate, *J. Geophys. Res. Atmospheres*, 101, 18667–18690, <https://doi.org/10.1029/96JD01221>, 1996.
- 590 Dolgorouky, C., Gros, V., Sarda-Esteve, R., Sinha, V., Williams, J., Marchand, N., Sauvage, S., Poulain, L., Sciare, J., and
591 Bonsang, B.: Total OH reactivity measurements in Paris during the 2010 MEGAPOLI winter campaign, *Atmospheric Chem. Phys.*,
592 12, 9593–9612, <https://doi.org/10.5194/acp-12-9593-2012>, 2012.
- 593 Dufour, G., Szopa, S., Harrison, J. J., Boone, C. D., and Bernath, P. F.: Seasonal variations of acetone in the upper troposphere–
594 lower stratosphere of the northern midlatitudes as observed by ACE-FTS, *J. Mol. Spectrosc.*, 323, 67–77,
595 <https://doi.org/10.1016/j.jms.2016.02.006>, 2016.
- 596 Elias, T., Szopa, S., Zahn, A., Schuck, T., Brenninkmeijer, C., Sprung, D., and Slemr, F.: Acetone variability in the upper
597 troposphere: analysis of CARIBIC observations and LMDz-INCA chemistry-climate model simulations, *Atmospheric Chem.*
598 *Phys.*, 11, 8053–8074, <https://doi.org/10.5194/acp-11-8053-2011>, 2011.
- 599 Fischbeck, G., Bönisch, H., Neumaier, M., Brenninkmeijer, C. A. M., Orphal, J., Brito, J., Becker, J., Sprung, D., van Velthoven,
'00 P. F. J., and Zahn, A.: Acetone–CO enhancement ratios in the upper troposphere based on 7 years of CARIBIC data: new insights
'01 and estimates of regional acetone fluxes, *Atmospheric Chem. Phys.*, 17, 1985–2008, <https://doi.org/10.5194/acp-17-1985-2017>,
'02 2017.

'03 Fischer, E. V., Jacob, D. J., Millet, D. B., Yantosca, R. M., and Mao, J.: The role of the ocean in the global atmospheric budget of
 '04 acetone, *Geophys. Res. Lett.*, 39, <https://doi.org/10.1029/2011GL050086>, 2012.

'05 Folberth, G. A., Hauglustaine, D. A., Lathière, J., and Brocheton, F.: Interactive chemistry in the Laboratoire de Météorologie
 '06 Dynamique general circulation model: model description and impact analysis of biogenic hydrocarbons on tropospheric chemistry,
 '07 *Atmospheric Chem. Phys.*, 6, 2273–2319, <https://doi.org/10.5194/acp-6-2273-2006>, 2006.

'08 Fujimori, S., Hasegawa, T., Masui, T., Takahashi, K., Herran, D. S., Dai, H., Hijioka, Y., and Kainuma, M.: SSP3: AIM
 '09 implementation of Shared Socioeconomic Pathways, *Glob. Environ. Change*, 42, 268–283,
 '10 <https://doi.org/10.1016/j.gloenvcha.2016.06.009>, 2017.

'11 Galbally, I., Lawson, S. J., Bentley, S., Gillett, R., Meyer, M., and Goldstein, A.: Volatile organic compounds in marine air at Cape
 '12 Grim, Australia, *Environ. Chem. - Env. CHEM*, 4, <https://doi.org/10.1071/EN07024>, 2007.

'13 Gelaro, R., McCarty, W., Suárez, M. J., Todling, R., Molod, A., Takacs, L., Randles, C. A., Darmenov, A., Bosilovich, M. G.,
 '14 Reichle, R., Wargan, K., Coy, L., Cullather, R., Draper, C., Akella, S., Buchard, V., Conaty, A., Silva, A. M. da, Gu, W., Kim, G.-
 '15 K., Koster, R., Lucchesi, R., Merkova, D., Nielsen, J. E., Partyka, G., Pawson, S., Putman, W., Rienecker, M., Schubert, S. D.,
 '16 Sienkiewicz, M., and Zhao, B.: The Modern-Era Retrospective Analysis for Research and Applications, Version 2 (MERRA-2),
 '17 *J. Clim.*, 30, 5419–5454, <https://doi.org/10.1175/JCLI-D-16-0758.1>, 2017.

'18 de Gouw, J., Warneke, C., Holzinger, R., Klüpfel, T., and Williams, J.: Inter-comparison between airborne measurements of
 '19 methanol, acetonitrile and acetone using two differently configured PTR-MS instruments, *Int. J. Mass Spectrom.*, 239, 129–137,
 '20 <https://doi.org/10.1016/j.jms.2004.07.025>, 2004.

'21 Guenther, A. B., Jiang, X., Heald, C. L., Sakulyanontvittaya, T., Duhl, T., Emmons, L. K., and Wang, X.: The Model of Emissions
 '22 of Gases and Aerosols from Nature version 2.1 (MEGAN2.1): an extended and updated framework for modeling biogenic
 '23 emissions, *Geosci. Model Dev.*, 5, 1471–1492, <https://doi.org/10.5194/gmd-5-1471-2012>, 2012.

'24 Guérette, É.-A., Paton-Walsh, C., Galbally, I., Molloy, S., Lawson, S., Kubistin, D., Buchholz, R., Griffith, D. W. T., Langenfelds,
 '25 R. L., Krummel, P. B., Loh, Z., Chambers, S., Griffiths, A., Keywood, M., Selleck, P., Dominick, D., Humphries, R., and Wilson,
 '26 S. R.: Composition of Clean Marine Air and Biogenic Influences on VOCs during the MUMBA Campaign, *Atmosphere*, 10, 383,
 '27 <https://doi.org/10.3390/atmos10070383>, 2019.

'28 Hoesly, R. M., Smith, S. J., Feng, L., Klimont, Z., Janssens-Maenhout, G., Pitkanen, T., Seibert, J. J., Vu, L., Andres, R. J., Bolt,
 '29 R. M., Bond, T. C., Dawidowski, L., Kholod, N., Kurokawa, J., Li, M., Liu, L., Lu, Z., Moura, M. C. P., O'Rourke, P. R., and
 '30 Zhang, Q.: Historical (1750–2014) anthropogenic emissions of reactive gases and aerosols from the Community Emissions Data
 '31 System (CEDS), *Geosci. Model Dev.*, 11, 369–408, <https://doi.org/10.5194/gmd-11-369-2018>, 2018.

'32 Hu, L., Millet, D. B., Kim, S. Y., Wells, K. C., Griffis, T. J., Fischer, E. V., Helmig, D., Hueber, J., and Curtis, A. J.: North
 '33 American acetone sources determined from tall tower measurements and inverse modeling, *Atmospheric Chem. Phys.*, 13, 3379–
 '34 3392, <https://doi.org/10.5194/acp-13-3379-2013>, 2013.

'35 Huang, X.-F., Zhang, B., Xia, S.-Y., Han, Y., Wang, C., Yu, G.-H., and Feng, N.: Sources of oxygenated volatile organic
 '36 compounds (OVOCs) in urban atmospheres in North and South China, *Environ. Pollut.*, 261, 114152,
 '37 <https://doi.org/10.1016/j.envpol.2020.114152>, 2020.

'38 Jacob, D. J., Field, B. D., Jin, E. M., Bey, I., Li, Q., Logan, J. A., Yantosca, R. M., and Singh, H. B.: Atmospheric budget of
 '39 acetone, *J. Geophys. Res. Atmospheres*, 107, ACH 5-1-ACH 5-17, <https://doi.org/10.1029/2001JD000694>, 2002.

'40 Johnson, M. T.: A numerical scheme to calculate temperature and salinity dependent air-water transfer velocities for any gas,
 '41 *Ocean Sci.*, 6, 913–932, <https://doi.org/10.5194/os-6-913-2010>, 2010.

'42 Kelley, M., Schmidt, G. A., Nazarenko, L. S., Bauer, S. E., Ruedy, R., Russell, G. L., Ackerman, A. S., Aleinov, I., Bauer, M.,
 '43 Bleck, R., Canuto, V., Cesana, G., Cheng, Y., Clune, T. L., Cook, B. I., Cruz, C. A., Genio, A. D. D., Elsaesser, G. S., Faluvegi,
 '44 G., Kiang, N. Y., Kim, D., Lacis, A. A., Leboissetier, A., LeGrande, A. N., Lo, K. K., Marshall, J., Matthews, E. E., McDermid,
 '45 S., Mezzuman, K., Miller, R. L., Murray, L. T., Oinas, V., Orbe, C., Garcia-Pando, C. P., Perlwitz, J. P., Puma, M. J., Rind, D.,
 '46 Romanou, A., Shindell, D. T., Sun, S., Tausnev, N., Tsigaridis, K., Tselioudis, G., Weng, E., Wu, J., and Yao, M.-S.: GISS-E2.1:
 '47 Configurations and Climatology, *J. Adv. Model. Earth Syst.*, 12, e2019MS002025, <https://doi.org/10.1029/2019MS002025>, 2020.

'48 Khan, M. A. H., Cooke, M. C., Utembe, S. R., Archibald, A. T., Maxwell, P., Morris, W. C., Xiao, P., Derwent, R. G., Jenkin, M.
 '49 E., Percival, C. J., Walsh, R. C., Young, T. D. S., Simmonds, P. G., Nickless, G., O'Doherty, S., and Shallcross, D. E.: A study of
 '50 global atmospheric budget and distribution of acetone using global atmospheric model STOCHEM-CRI, *Atmos. Environ.*, 112,
 '51 269–277, <https://doi.org/10.1016/j.atmosenv.2015.04.056>, 2015.

'52 Koch, D., Jacob, D., Tegen, I., Rind, D., and Chin, M.: Tropospheric sulfur simulation and sulfate direct radiative forcing in the
 '53 Goddard Institute for Space Studies general circulation model, *J. Geophys. Res. Atmospheres*, 104, 23799–23822,
 '54 <https://doi.org/10.1029/1999JD900248>, 1999.

'55 Langford, B., Nemitz, E., House, E., Phillips, G. J., Famulari, D., Davison, B., Hopkins, J. R., Lewis, A. C., and Hewitt, C. N.:
 '56 Fluxes and concentrations of volatile organic compounds above central London, UK, *Atmospheric Chem. Phys.*, 10, 627–645,
 '57 <https://doi.org/10.5194/acp-10-627-2010>, 2010.

'58 Legrand, M., Gros, V., Preunkert, S., Sarda-Estève, R., Thierry, A.-M., Pépy, G., and Jourdain, B.: A reassessment of the budget
 '59 of formic and acetic acids in the boundary layer at Dumont d'Urville (coastal Antarctica): The role of penguin emissions on the
 '60 budget of several oxygenated volatile organic compounds, *J. Geophys. Res. Atmospheres*, 117,
 '61 <https://doi.org/10.1029/2011JD017102>, 2012.

'62 Lewis, A. C., Hopkins, J. R., Carpenter, L. J., Stanton, J., Read, K. A., and Pilling, M. J.: Sources and sinks of acetone, methanol,
 '63 and acetaldehyde in North Atlantic marine air, *Atmospheric Chem. Phys.*, 5, 1963–1974, <https://doi.org/10.5194/acp-5-1963-2005>,
 '64 2005.

'65 Li, K., Li, J., Tong, S., Wang, W., Huang, R.-J., and Ge, M.: Characteristics of wintertime VOCs in suburban and urban Beijing:
 '66 concentrations, emission ratios, and festival effects, *Atmospheric Chem. Phys.*, 19, 8021–8036, <https://doi.org/10.5194/acp-19-8021-2019>, 2019.

'68 Liss, P. S. and Slater, P. G.: Flux of Gases across the Air-Sea Interface, *Nature*, 247, 181–184, <https://doi.org/10.1038/247181a0>,
 '69 1974.

'70 Marandino, C. A., Bruyn, W. J. D., Miller, S. D., Prather, M. J., and Saltzman, E. S.: Oceanic uptake and the global atmospheric
 '71 acetone budget, *Geophys. Res. Lett.*, 32, <https://doi.org/10.1029/2005GL023285>, 2005.

'72 van Marle, M. J. E., Kloster, S., Magi, B. I., Marlon, J. R., Daniiau, A.-L., Field, R. D., Arneth, A., Forrest, M., Hantson, S.,
 '73 Kehrwald, N. M., Knorr, W., Lasslop, G., Li, F., Mangeon, S., Yue, C., Kaiser, J. W., and van der Werf, G. R.: Historic global
 '74 biomass burning emissions for CMIP6 (BB4CMIP) based on merging satellite observations with proxies and fire models (1750–
 '75 2015), *Geosci. Model Dev.*, 10, 3329–3357, <https://doi.org/10.5194/gmd-10-3329-2017>, 2017.

'76 Neu, J. L., Prather, M. J., and Penner, J. E.: Global atmospheric chemistry: Integrating over fractional cloud cover, *J. Geophys.*
 '77 *Res. Atmospheres*, 112, 2006JD008007, <https://doi.org/10.1029/2006JD008007>, 2007.

'78 O'Rourke, P. R., Smith, S. J., Mott, A., Ahsan, H., McDuffie, E. E., Crippa, M., Klimont, Z., McDonald, B., Wang, S., Nicholson,
 '79 M. B., Feng, L., and Hoesly, R. M.: CEDS v_2021_04_21 Release Emission Data, <https://doi.org/10.5281/zenodo.4741285>, 2021.

'80 Read, K. A., Carpenter, L. J., Arnold, S. R., Beale, R., Nightingale, P. D., Hopkins, J. R., Lewis, A. C., Lee, J. D., Mendes, L., and
 '81 Pickering, S. J.: Multiannual Observations of Acetone, Methanol, and Acetaldehyde in Remote Tropical Atlantic Air: Implications
 '82 for Atmospheric OVOC Budgets and Oxidative Capacity, *Environ. Sci. Technol.*, 46, 11028–11039,
 '83 <https://doi.org/10.1021/es302082p>, 2012.

'84 Riahi, K., van Vuuren, D. P., Kriegler, E., Edmonds, J., O'Neill, B. C., Fujimori, S., Bauer, N., Calvin, K., Dellink, R., Fricko, O.,
 '85 Lutz, W., Popp, A., Cuaresma, J. C., Ke, S., Leimbach, M., Jiang, L., Kram, T., Rao, S., Emmerling, J., Ebi, K., Hasegawa, T.,
 '86 Havlik, P., Humpenöder, F., Da Silva, L. A., Smith, S., Stehfest, E., Bosetti, V., Eom, J., Gernaat, D., Masui, T., Rogelj, J., Strefler,
 '87 J., Drouet, L., Krey, V., Luderer, G., Harnsen, M., Takahashi, K., Baumstark, L., Doelman, J. C., Kainuma, M., Klimont, Z.,
 '88 Marangoni, G., Lotze-Campen, H., Obersteiner, M., Tabeau, A., and Tavoni, M.: The Shared Socioeconomic Pathways and their
 '89 energy, land use, and greenhouse gas emissions implications: An overview, *Glob. Environ. Change*, 42, 153–168,
 '90 <https://doi.org/10.1016/j.gloenvcha.2016.05.009>, 2017.

'91 Sander, R.: *Compilation of Henry's Law Constants for Inorganic and Organic Species of Potential Importance in Environmental*
 '92 *Chemistry*, 1999.

93 Sander, S. P., J. Abbatt, J. R. Barker, J. B. Burkholder, R. R. Friedl, D. M. Golden, R. E. Huie, C. E. Kolb, M. J. Kurylo, G. K.
 94 Moortgat, V. L. Orkin, and P. H. Wine: Chemical Kinetics and Photochemical Data for Use in Atmospheric Studies Evaluation
 95 No. 17, JPL Publication 10-6, Jet Propulsion Laboratory, Pasadena, 2011.

96 Schade, G. W. and Goldstein, A. H.: Seasonal measurements of acetone and methanol: Abundances and implications for
 97 atmospheric budgets, *Glob. Biogeochem. Cycles*, 20, <https://doi.org/10.1029/2005GB002566>, 2006.

98 Shindell, D. T., Grenfell, J. L., Rind, D., Grewe, V., and Price, C.: Chemistry-climate interactions in the Goddard Institute for
 99 Space Studies general circulation model: 1. Tropospheric chemistry model description and evaluation, *J. Geophys. Res.*
 100 *Atmospheres*, 106, 8047–8075, <https://doi.org/10.1029/2000JD900704>, 2001.

101 Shindell, D. T., Faluvegi, G., and Bell, N.: Preindustrial-to-present-day radiative forcing by tropospheric ozone from improved
 102 simulations with the GISS chemistry-climate GCM, *Atmospheric Chem. Phys.*, 3, 1675–1702, [https://doi.org/10.5194/acp-3-1675-](https://doi.org/10.5194/acp-3-1675-2003)
 103 2003, 2003.

104 Singh, H., Chen, Y., Tabazadeh, A., Fukui, Y., Bey, I., Yantosca, R., Jacob, D., Arnold, F., Wohlfrom, K., Atlas, E., Flocke, F.,
 105 Blake, D., Blake, N., Heikes, B., Snow, J., Talbot, R., Gregory, G., Sachse, G., Vay, S., and Kondo, Y.: Distribution and fate of
 106 selected oxygenated organic species in the troposphere and lower stratosphere over the Atlantic, *J. Geophys. Res. Atmospheres*,
 107 105, 3795–3805, <https://doi.org/10.1029/1999JD900779>, 2000.

108 Singh, H. B., O'Hara, D., Herlth, D., Sachse, W., Blake, D. R., Bradshaw, J. D., Kanakidou, M., and Crutzen, P. J.: Acetone in the
 109 atmosphere: Distribution, sources, and sinks, *J. Geophys. Res. Atmospheres*, 99, 1805–1819, <https://doi.org/10.1029/93JD00764>,
 110 1994.

111 Singh, H. B., Tabazadeh, A., Evans, M. J., Field, B. D., Jacob, D. J., Sachse, G., Crawford, J. H., Shetter, R., and Brune, W. H.:
 112 Oxygenated volatile organic chemicals in the oceans: Inferences and implications based on atmospheric observations and air-sea
 113 exchange models, *Geophys. Res. Lett.*, 30, <https://doi.org/10.1029/2003GL017933>, 2003.

114 Singh, H. B., Salas, L. J., Chatfield, R. B., Czech, E., Fried, A., Walega, J., Evans, M. J., Field, B. D., Jacob, D. J., Blake, D.,
 115 Heikes, B., Talbot, R., Sachse, G., Crawford, J. H., Avery, M. A., Sandholm, S., and Fuelberg, H.: Analysis of the atmospheric
 116 distribution, sources, and sinks of oxygenated volatile organic chemicals based on measurements over the Pacific during TRACE-
 117 P, *J. Geophys. Res. Atmospheres*, 109, <https://doi.org/10.1029/2003JD003883>, 2004.

118 Solberg, S., Dye, C., Schmidbauer, N., Herzog, A., and Gehrig, R.: Carbonyls and nonmethane hydrocarbons at rural European
 119 sites from the mediterranean to the arctic, *J. Atmospheric Chem.*, 25, 33–66, <https://doi.org/10.1007/BF00053285>, 1996.

120 Thompson, C. R., Wofsy, S. C., Prather, M. J., Newman, P. A., Hanisco, T. F., Ryerson, T. B., Fahey, D. W., Apel, E. C., Brock,
 121 C. A., Brune, W. H., Froyd, K., Katich, J. M., Nicely, J. M., Peischl, J., Ray, E., Veres, P. R., Wang, S., Allen, H. M., Asher, E.,
 122 Bian, H., Blake, D., Bourgeois, I., Budney, J., Bui, T. P., Butler, A., Campuzano-Jost, P., Chang, C., Chin, M., Commane, R.,
 123 Correa, G., Crounse, J. D., Daube, B., Dibb, J. E., DiGangi, J. P., Diskin, G. S., Dollner, M., Elkins, J. W., Fiore, A. M., Flynn, C.
 124 M., Guo, H., Hall, S. R., Hannun, R. A., Hills, A., Hints, E. J., Hodzic, A., Hornbrook, R. S., Huey, L. G., Jimenez, J. L., Keeling,
 125 R. F., Kim, M. J., Kupe, A., Lacey, F., Lait, L. R., Lamarque, J.-F., Liu, J., McKain, K., Meinardi, S., Miller, D. O., Montzka, S.
 126 A., Moore, F. L., Morgan, E. J., Murphy, D. M., Murray, L. T., Nault, B. A., Neuman, J. A., Nguyen, L., Gonzalez, Y., Rollins,
 127 A., Rosenlof, K., Sargent, M., Schill, G., Schwarz, J. P., Clair, J. M. S., Steenrod, S. D., Stephens, B. B., Strahan, S. E., Strode, S.
 128 A., Sweeney, C., Thames, A. B., Ullmann, K., Wagner, N., Weber, R., Weinzierl, B., Wennberg, P. O., Williamson, C. J., Wolfe,
 129 G. M., and Zeng, L.: The NASA Atmospheric Tomography (ATom) Mission: Imaging the Chemistry of the Global Atmosphere,
 130 *Bull. Am. Meteorol. Soc.*, 103, E761–E790, <https://doi.org/10.1175/BAMS-D-20-0315.1>, 2022.

131 Tsigaridis, K. and Kanakidou, M.: Global modelling of secondary organic aerosol in the troposphere: a sensitivity analysis, *Atmos*
 132 *Chem Phys*, 2003.

133 Wang, S., Apel, E. C., Schwantes, R. H., Bates, K. H., Jacob, D. J., Fischer, E. V., Hornbrook, R. S., Hills, A. J., Emmons, L. K.,
 134 Pan, L. L., Honomichl, S., Tilmes, S., Lamarque, J.-F., Yang, M., Marandino, C. A., Saltzman, E. S., Bruyn, W. de, Kameyama,
 135 S., Tanimoto, H., Omori, Y., Hall, S. R., Ullmann, K., Ryerson, T. B., Thompson, C. R., Peischl, J., Daube, B. C., Commane, R.,
 136 McKain, K., Sweeney, C., Thames, A. B., Miller, D. O., Brune, W. H., Diskin, G. S., DiGangi, J. P., and Wofsy, S. C.: Global
 137 Atmospheric Budget of Acetone: Air-Sea Exchange and the Contribution to Hydroxyl Radicals, *J. Geophys. Res. Atmospheres*,
 138 125, e2020JD032553, <https://doi.org/10.1029/2020JD032553>, 2020.

139 Warneke, C. and de Gouw, J. A.: Organic trace gas composition of the marine boundary layer over the northwest Indian Ocean in
 140 April 2000, *Atmos. Environ.*, 35, 5923–5933, [https://doi.org/10.1016/S1352-2310\(01\)00384-3](https://doi.org/10.1016/S1352-2310(01)00384-3), 2001.

141 Weimer, M., Schröter, J., Eckstein, J., Deetz, K., Neumaier, M., Fischbeck, G., Hu, L., Millet, D. B., Rieger, D., Vogel, H., Vogel,
142 B., Reddmann, T., Kirner, O., Ruhnke, R., and Braesicke, P.: An emission module for ICON-ART 2.0: implementation and
143 simulations of acetone, *Geosci. Model Dev.*, 10, 2471–2494, <https://doi.org/10.5194/gmd-10-2471-2017>, 2017.

144 Wesely, M. L. and Hicks, B. B.: Some Factors that Affect the Deposition Rates of Sulfur Dioxide and Similar Gases on Vegetation,
145 *J. Air Pollut. Control Assoc.*, 27, 1110–1116, <https://doi.org/10.1080/00022470.1977.10470534>, 1977.

146 Yoshino, A., Nakashima, Y., Miyazaki, K., Kato, S., Suthawaree, J., Shimo, N., Matsunaga, S., Chatani, S., Apel, E., Greenberg,
147 J., Guenther, A., Ueno, H., Sasaki, H., Hoshi, J., Yokota, H., Ishii, K., and Kajii, Y.: Air quality diagnosis from comprehensive
148 observations of total OH reactivity and reactive trace species in urban central Tokyo, *Atmos. Environ.*, 49, 51–59,
149 <https://doi.org/10.1016/j.atmosenv.2011.12.029>, 2012.

150 Yuan, B., Hu, W. W., Shao, M., Wang, M., Chen, W. T., Lu, S. H., Zeng, L. M., and Hu, M.: VOC emissions, evolutions and
151 contributions to SOA formation at a receptor site in eastern China, *Atmospheric Chem. Phys.*, 13, 8815–8832,
152 <https://doi.org/10.5194/acp-13-8815-2013>, 2013.

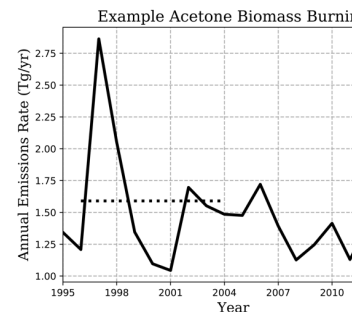
153 Zhou, X. and Mopper, K.: Apparent partition coefficients of 15 carbonyl compounds between air and seawater and between air
154 and freshwater; implications for air-sea exchange, *Environ. Sci. Technol.*, 24, 1864–1869, <https://doi.org/10.1021/es00082a013>,
155 1990.

158

Moved up [1]: Table 1. Sensitivity studies conducted to specific parameter afforded the model. Simulation names, as

Deleted: Tables and Figures
Table 1. Sensitivity studies conducted to observe the leverage a specific parameter afforded the model. Simulation names. ... [1]

Formatted: Heading 1

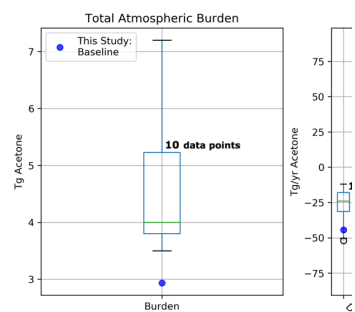


Deleted:

Deleted:

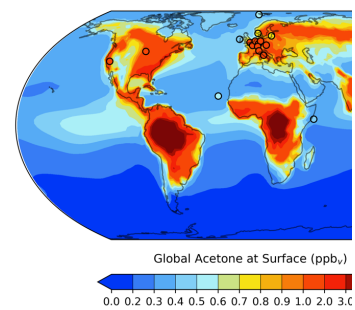
Deleted: Figure 1. Illustration of interannual variability of NMVOC-C3H6 biomass burning emissions of van Marle et al., (2017) (solid line), used as acetone emissions in our simula... [2]

Deleted:



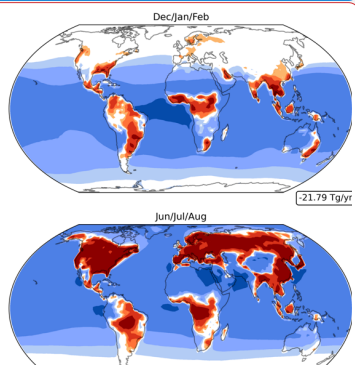
Deleted: ... [3]

Deleted:



Deleted: ... [4]

Deleted:



Page 29: [1] Deleted Alexandra Rivera 10/25/23 9:52:00 AM

Page 29: [2] Deleted Microsoft Office User 10/25/23 9:38:00 AM

Page 29: [3] Deleted Microsoft Office User 10/25/23 9:39:00 AM

Page 29: [4] Deleted Microsoft Office User 10/25/23 9:41:00 AM

Page 29: [5] Deleted Microsoft Office User 10/25/23 9:42:00 AM

Page 29: [6] Deleted Microsoft Office User 10/25/23 9:43:00 AM

Page 29: [7] Deleted Microsoft Office User 10/25/23 9:43:00 AM

Page 29: [8] Deleted Microsoft Office User 10/25/23 9:43:00 AM

Page 29: [9] Deleted Alexandra Rivera 11/6/23 6:31:00 PM